

Phase equilibria modelling of residual migmatites and granulites: an evaluation of the melt-reintegration approach

Omar Bartoli

¹*Department of Geosciences, University of Padova, Italy*

Corresponding author mail id: omar.bartoli@unipd.it

Short title: Evaluating melt-reintegration approach

ABSTRACT

Suprasolidus continental crust is prone to loss and redistribution of anatectic melt to shallow crustal levels. These processes ultimately lead to differentiation of the continental crust. The majority of granulite facies rocks worldwide has experienced melt loss and the reintegration of melt is becoming an increasingly popular approach to reconstruct the prograde history of melt-depleted rocks by means of phase equilibria modelling. It involves the stepwise down-temperature reintegration of a certain amount of melt into the residual bulk composition along an inferred P - T path, and various ways of calculating and reintegrating melt compositions have been developed and applied. Here different melt-reintegration approaches are tested using El Hoyazo granulitic enclaves (SE Spain), and Mt. Stafford residual migmatites (central Australia). Various sets of P - T pseudosections were constructed progressing step by step, to lower temperatures along the inferred P - T paths. Melt-reintegration was done following one-step and multi-step procedures proposed in the literature. For El Hoyazo granulites, modelling was also performed reintegrating the measured melt inclusions and matrix glass compositions and considering the melt amounts inferred by mass-balance calculations. The overall topology of phase diagrams is pretty similar, suggesting that, in spite of the different methods adopted, reintegrating a certain amount of melt can be sufficient to reconstruct a plausible prograde history (i.e., melting conditions and reactions, and melt productivity) of residual migmatites and granulites. However, significant underestimations of melt productivity may occur and have to be taken into account when a melt-reintegration approach is applied to highly residual ($\text{SiO}_2 < 55$ wt.%) rocks, or to rocks for which H_2O retention from subsolidus conditions is high (such as in the case of rapid crustal melting triggered by mafic magma underplating).

Key words: residual migmatite, granulite, melt loss, melt-reintegration, melt productivity

This article has been accepted for publication and undergone full peer review but has not been through the copyediting, typesetting, pagination and proofreading process, which may lead to differences between this version and the Version of Record. Please cite this article as doi: 10.1111/jmg.12261

This article is protected by copyright. All rights reserved.

1 INTRODUCTION

Crustal anatexis and extraction and ascent of anatectic melts to upper crustal levels represent the main agents of differentiation of the continental crust (Brown, 2010a, 2013; Sawyer, Cesare, & Brown, 2011), and deeply affect the tectonic evolution of orogens (Brown, 2001; Handy, Mulch, Rosenau, & Rosenberg, 2001; Yakymchuk & Brown, 2014a). Overall, the suprasolidus crust can be considered an unconditionally open system, because it is prone to drainage of melt to shallow crustal levels to form anatectic granites (Sawyer et al., 2011; Yakymchuk & Brown, 2014a). At a more local scale, however, melt loss is expected not to be continuous (Brown, 2013). Rather, the process of melt extraction is likely to be cyclic, with melt loss occurring when a critical threshold is reached (i.e., the suprasolidus crust can be assumed as a conditionally open system; Laporte, Rapaille & Provost, 1997; Handy, Mulch, Rosenau, & Rosenberg, 2001; Maaløe & Scheie, 1982; Sawyer, 1994; Vigneresse, Barbey, & Cuney, 1996; Yakymchuk & Brown, 2014a).

Migmatites can represent zones of melt generation, melt transfer or melt accumulation (Brown, 2010a; Brown et al., 2016; Carvalho, Sawyer, & Janasi, 2016; Morfin, Sawyer, & Bandyayera, 2014; Sawyer, 2008). Granulites, instead, are considered to be the residuum of melting process (Vielzeuf, Clemens, Pin, & Moinet, 1990; White & Powell, 2002). Most granulitic terranes experienced net loss of anatectic melt as suggested by preservation of anhydrous peak mineral assemblages (White & Powell, 2002), residual bulk rock compositions (Sawyer, 1991; Solar & Brown, 2001), and field structures associated with a volume reduction (Bons, Druguet, Castaño, & Elburg, 2008; Brown, 2010a; Yakymchuk, Brown, Ivanic, & Korhonen, 2013). Progress in investigation of high-grade, partially-melted crystalline basements has been made in the last decades by phase equilibria modelling based on large, internally consistent thermodynamic datasets (e.g. Johnson, White, & Powell, 2008; Palin, Weller, Waters, & Dyck, 2016a; White, Powell, & Holland, 2007; White, Stevens, Johnson, 2011; White, Palin, & Green, 2017; and references therein), though there are still opportunities for further and significant enhancements (Brown, 2013; White et al., 2011).

The lack of an appropriate pre-melt-loss protolith composition would have made impossible to recover the entire prograde and melt production history of melt-depleted rocks by means of phase equilibria modelling. This issue was circumvented by reintegrating a certain amount of melt to the residuum composition and by performing phase equilibria modelling of the new model protolith composition to reconstruct the probable prograde history (see White, Powell, & Halpin, 2004). The melt-reintegration approach has become an increasingly routine method among metamorphic petrologists and various ways of calculating and reintegrating the extracted melt have been developed and applied (Anderson, Kelsey, Hand, & Collins, 2013; Boger, White, & Schulte, 2012; Cai et al., 2014, 2016; Chen, ye, Liu, & Sun, 2008; Diener, White, & Powell, 2008; Diener, White, Link, Dreyer, & Moodley, 2013; Diener, White, & Hudson, 2014; Dumond, Goncalves, Williams, & Jercinovic, 2015; Fitzherbert, 2015; Groppo, Rubatto, Rolfo, & Lombardo, 2010; Groppo, Rolfo, & Indares, 2012; Groppo, Rolfo, & Mosca, 2013; Guilmette, Indares, & Hébert, 2011; Hallett & Spear, 2014; Hasalová et al., 2008; Jiang et al., 2015; Kelsey & Hand, 2014; Kohn, 2014; Korhonen, Brown, Clark, & Bhattacharya, 2013; Indares, White, & Powell, 2008; Lasalle & Indares, 2014; McGee, Giles, Kelsey, & Collins, 2010; Morrissey, Hand, Kelsey, & Wade, 2016a; Nahodilová, Faryad, Dolejš, Tropper, & Konzett, 2011; Nicoli, Stevens, Moyen, & Frei, 2015; Palin et al., 2013; Redler, White, & Johnson, 2013; Shrestha, Larson, Guilmette, & Smit, 2017; Skrzypek, Štípská, & Cocherie, 2012; Štípská, Schulmann, & Powell, 2008; Taylor, Nicoli, Stevens, Frei, & Moyen, 2014; Tian, Zhang, & Dong, 2016; Tucker, Hand, Kelsey, & Dutch, 2015; Wang & Guo, 2017; White et al., 2004; Yakymchuk et al., 2015; Yin

et al., 2014; Zhang et al., 2015; Zou et al., 2017). Furthermore, the reconstruction of a plausible protolith composition is essential to assess the likely melt productivity of rocks (White et al., 2004) which, in turn, allows the potential role of loss and redistribution of melt in the evolution of the deeper crust to be explored (Diener & Fagereng, 2014; Diener et al., 2014; Korhonen, Saito, Brown, & Siddoway, 2010; Korhonen et al., 2013; Morrissey, Hand, Lane, Kelsey, Dutch, 2016b; Yakymchuck & Brown, 2014; White & Powell, 2010).

In this contribution, the different melt-reintegration approaches proposed in the literature are, firstly, reviewed. Then, results of the phase equilibria modelling of the El Hoyazo granulitic enclaves (SE Spain) and the Mt. Stafford migmatites (central Australia) are presented and discussed. These two case studies present different advantages and limitations. The El Hoyazo enclaves are considered to be fragments of the residual, partially melted metapelitic continental crust beneath the Neogene Volcanic Province of SE Spain (Cesare, 2008). Because the P - T conditions of melting, the topology of melting reactions, and, most important, the composition and amount of melts produced and lost along the prograde path are well-constrained by a combination of different methods (e.g., microstructures, bulk rock geochemistry, thermobarometry, mass balance and geochemical characterization of melt inclusions), the El Hoyazo granulites can be considered ideal candidates to test melt-reintegration approaches. However, the link between the residual enclaves and their protolith is not explicit.

On the other hand, Mt. Stafford rocks represent a well-studied metamorphic sequence from greenschist- to granulite-facies conditions. Here the protolith composition is well-known and the melting history is recorded in detail (White, Powell, & Clarke, 2003; and references therein). The disadvantage is that melt inclusions have not been documented in Mt. Stafford migmatites and, therefore, only calculated melt compositions can be reintegrated. Thus, examples of melt-reintegration to reconstruct the prograde P - T evolution are presented and discussed. Two bulk rock compositions showing different degrees of melt-depletion are selected to test the feasibility of melt-reintegration approach.

2 MELT-REINTEGRATION PROCEDURES PROPOSED IN THE LITERATURE

In previous studies from the literature, the P - T conditions at which melt compositions have been calculated and the number of reintegration steps vary from study to study. Rocks are generally thought to be H_2O -saturated at the solidus as a consequence of subsolidus dehydration reactions (Thompson & Connolly, 1995), and the appearance of a H_2O -saturated solidus at <700 °C has been generally used to determine the amount of melt to add back to the measured bulk rock composition (e.g., Guilmette et al., 2011; Indares et al., 2008; Korhonen et al., 2013; Lasalle & Indares, 2014; Palin et al., 2013; Redler et al., 2013; Skrzypek et al., 2012; Zou et al., 2017).

2.1 Single-step approach

In some works, the simplest case of melt loss, and therefore of melt-reintegration, was assumed to occur in one step (e.g., Guilmette et al., 2011; Hallet & Spear, 2014; Indares et al., 2008; Lasalle & Indares, 2014; Tian et al., 2016; Zhang et al., 2015; Zou et al., 2017). Melt compositions were calculated and reintegrated in different ways, such as at the intersection of the solidus for the residual composition with a presumed prograde P - T path (Indares et al., 2008), at the peak P - T conditions (Groppo et al., 2013) or at the hypothetical conditions at which melt was lost (Groppo et al., 2012). Recently, Wang & Guo (2017) reintegrated an average measured bulk composition of leucosomes found in the investigated area.

2.2 Multi-step approach

More refined approaches consist of a series of melt-reintegration operations rather than reintegration in one step (e.g., Korhonen et al., 2013; White et al., 2004). In the original method proposed by White et al. (2004), melt was added back at conditions of the original solidus calculated with the observed bulk composition until melt persisted to lower temperatures. The procedure was repeated so that the lower temperature boundary of each phase assemblage field involves the loss of a solid phase rather than melt, until a free fluid was present beyond the solidus (see also Yakymchuck et al., 2015). In this method the melt composition is also updated every time a new assemblage field is encountered. In this way the composition of the integrated melt changes to lower temperature, to mimic the compositional evolution of melt produced during prograde metamorphism.

Korhonen et al. (2013) proposed a different multi-step approach. They assumed 7 vol.% as the melt amount at which melt loss occurs in nature according to experiments (see Rosenberg & Handy, 2005) and that melt did not drain completely, but a small volume (~1 vol.%) likely remained among grain boundaries. Therefore, the modelling performed by these authors involved backtracking down temperature along a schematic prograde path to a P - T point where the amount of melt remaining in the phase assemblage field is 1 vol.% (~1 wt.%). At this point, 6 vol.% (~5 wt.%) melt of the composition in equilibrium with the assemblage at these P - T conditions was reintegrated into the bulk chemical composition, resulting in 7 vol.% (~6 wt.%) total melt at this P - T condition. The procedure was repeated until a H_2O -saturated solidus appeared between 650 and 690 °C (Dumond et al., 2015; Korhonen et al., 2013). This method is the inverse of that adopted by Yakymchuk & Brown (2014a, b) and Palin et al. (2016b) to model multiple melt loss events.

2.3 T - M_{melt} section approach

Anderson et al. (2013) proposed an alternative method. The procedure consisted of employing a T - M_{melt} section at appropriate pressure for the investigated rock, constructed using the residual bulk composition (M_0) and the composition of an average silicate melt (M_1). The latter was determined using published leucogranite compositions. Anderson et al. (2013) suggested that the appropriate bulk composition has to be constrained by the following factors: “(i) the composition should intersect the peak mineral assemblage field interpreted from the rock; (ii) the composition should replicate to a close approximation the abundance of biotite and the composition of a phase with robust mineral chemistry (where part of the peak assemblage) and (iii) the composition should not pass through assemblage fields that have H_2O as a free fluid phase”. The obtained bulk composition was then used to calculate a P - T pseudosection considered to be appropriate to peak conditions (Anderson et al., 2013).

Because the selected composition does not pass through mineral assemblage fields containing H_2O as a free fluid phase in the T - M_{melt} section (see above), the solidus commonly appears at > 750 °C in the new P - T pseudosection (Anderson et al., 2013). Therefore, this approach does not allow reconstruction of the entire prograde history (i.e., from subsolidus to peak conditions) of melt-depleted rocks.

3 GEOLOGICAL AND PETROLOGICAL BACKGROUND

3.1 El Hoyazo granulitic enclaves (SE Spain)

The El Hoyazo volcano belongs to the Neogene Volcanic Province (NVP) of SE Spain (Cesare, Salvioli Mariani, & Venturelli, 1997). Volcanism is mostly late orogenic and occurred in an extensional setting (Zeck, Kristensen, & Williams, 1998). Underplating of mantle-derived basic magmas caused a rapid, almost isobaric heating (Figure 1a) and partial melting of the metasedimentary crust (Álvarez-Valero & Kriegsman, 2007; Cesare & Maineri, 1999). The lava dome comprises strongly peraluminous Grt- and Crd-bearing dacites (extrusion age of 6.33 ± 0.15 Ma; Zeck & Williams, 2002), which host abundant anatectic metapelitic enclaves (Figure S1a) (Zeck, 1992). They have been grouped in three main types: Bt–Grt–Sil, Spl–Crd and Qtz–Crd (Zeck, 1970, 1992). Mass balance calculations indicate that El Hoyazo enclaves represent the residuum after anatexis of graphitic metapelites and extraction of 40–60 wt.% granitic melt, contaminated by mafic magmas (Benito et al., 1999) and now represented by the host dacite (Cesare, 2008; Cesare & Maineri, 1999; Cesare et al., 1997).

Different lines of evidence (e.g., thin layers of interstitial rhyolitic glass parallel to the main foliation and surrounding melt inclusion-bearing porphyroblasts) indicate that melting in these rocks occurred when the crust was deforming as a coherent body, in a regional-scale process and not when enclaves were incorporated into the rising dacitic magma (Acosta-Vigil et al., 2010; Acosta-Vigil, Buick, Cesare, London, & Morgan, 2012; Cesare, 2000, 2008; Cesare & Gómez-Pugnaire, 2001). After the peak of metamorphism and anatexis (at 850 ± 50 °C and 5–7 kbar in the case of Bt–Grt–Sil enclaves), these rocks underwent a decompression event, most probably following incorporation in the host dacite magma (Figure 1a; Álvarez-Valero, Cesare, & Kriegsman, 2007).

Owing to the rapid cooling during extrusion of the host lava, the residual anatectic melt is preserved as glass within the enclaves. Silicate glass is present as melt inclusions (MI) within rock-forming minerals (Figure S1b,c) and in the matrix of the enclaves (Figure S1d). Melt inclusions are often distributed in zonal arrangements (Figure S1b) which reflect the progressive growth of the host mineral (Acosta-Vigil, Cesare, London, & Morgan, 2007) and which represent the most compelling evidence for primary trapping (Acosta-Vigil et al., 2016; Bartoli, Cesare, Remusat, Acosta-Vigil, & Poli, 2014; Bartoli, Acosta-Vigil, Ferrero, & Cesare, 2016a; Cesare, Acosta-Vigil, Ferrero, & Bartoli, O., 2011; Cesare, Acosta-Vigil, Bartoli, & Ferrero, 2015; Ferrero et al., 2012).

3.1.2 Bt–Grt–Sil enclaves

This contribution is focused on the Bt–Grt–Sil enclaves (Figure S1a). These samples contain a well-preserved granulite facies Bt–Grt–Crd–Sil–Pl–Kfs–Ilm quartz-free assemblage; accessory phases include graphite, apatite, monazite and zircon (Acosta-Vigil et al., 2010; Cesare et al., 1997). The bulk composition is highly residual ($\text{SiO}_2 \sim 45$ wt.%, $\text{Al}_2\text{O}_3 \sim 30$ wt.%, $\text{FeO} \sim 13$ wt.%; Table 1). The reader may refer to Cesare et al. (1997), Cesare (2008) and Acosta-Vigil et al. (2010, 2012) for additional details on the petrography and mineral chemistry of these rocks.

Undevitrified glass has been chemically investigated both within plagioclase and garnet where it is present as small (~ 5 – 30 μm) primary MI (Figure S1b,c) and in the rock matrix (Figure S1d) where it often occurs along foliation planes (e.g., Acosta-Vigil et al., 2007, 2010, 2012; Cesare et al., 1997; Cesare, Maineri, Baron Toaldo, Pedron, & Acosta-Vigil, 2007). The latter is the equivalent of leucosomes in regional migmatites and granulites.

The glass has a peraluminous leucogranitic composition ($\text{SiO}_2 \sim 70 \text{ wt.}\%$; $\text{FeO}+\text{MgO}+\text{TiO}_2 < 2 \text{ wt.}\%$; $\text{ASI} \sim 1.1\text{-}1.2$; Acosta-Vigil et al. 2007; Cesare et al. 2015) in agreement with melting of a metapelitic protolith. Glass H_2O contents have been directly measured by NanoSIMS (see also Bartoli et al., 2014).

Melt inclusions within plagioclase and garnet have been investigated in detail by Acosta-Vigil et al. (2007, 2010, 2012). Regarding trace elements, MI in both minerals are rich in those elements partially to totally controlled by muscovite, e.g., Li, Cs, B (Acosta-Vigil et al., 2010). Conversely, the matrix glass is characterized by lower concentrations of large ion lithophile elements (LILE) and higher contents of first row transition elements (FRTE), Sc, V, Cr, Co, Ni, high field strength elements (HFSE) Y, Zr, Th, REE, and higher Rb/Cs and Rb/Li, indicating the involvement of biotite in the melting reaction (Acosta-Vigil et al., 2010, 2012). Acosta-Vigil et al. (2010) calculated the zircon and monazite saturation temperatures and obtained an increase in temperature from 670-700 °C in MI in plagioclase, to 700-750 °C in MI in garnet, and up to 810 °C for matrix glass (Figure 1a). Because the analyzed melts seem to be undersaturated to some extent in the accessory phases (Acosta-Vigil et al. 2012), the obtained temperatures have to be considered as minimum estimates (Acosta-Vigil et al. 2010; Miller, McDowell, & Mapes, 2003). Álvarez-Valero & Waters (2010) reported a maximum temperature of 770 °C for the matrix melt.

From all the above observations, it was concluded that MI in plagioclase reflect the earliest granitic melts produced by fluid-present evolving rapidly to fluid-absent muscovite melting, whereas MI in garnet were produced simultaneously to slightly later via fluid-absent melting of muscovite. In contrast, the matrix melt represents the latest melt produced by biotite dehydration-melting up to peak conditions (Figure 1a). Acosta-Vigil et al. (2010) modelled the amounts of melt formed during prograde heating and obtained that ~20 wt.% of anatectic melt was produced by fluid- present muscovite melting, ~25 wt.% by muscovite dehydration-melting and ~15 wt.% by biotite dehydration-melting (Figure 1a).

3.2 Mount Stafford rocks (central Australia)

Mount Stafford is located in central Australia, within the southern part of the Northern Territory. This area is part of the Proterozoic Arunta Region and is dominated by Paleoproterozoic metasedimentary rocks –Mt. Stafford Beds– and large deformed granitoids (Mt. Stafford granite; Compston, 1995; Vernon, Clarke, & Collins, 1990). Metasedimentary rocks consist of metapelite interbedded with metapsammite layers and cordierite granofels (Greenfield, Clarke, Bland, & Clark, 1996), and have been interpreted to represent parts of a turbidite succession (Stewart, Shaw, & Black, 1984). A sequence of five metamorphic zones that range from greenschist- to granulite-facies has been recognized and mapped over a distance of 10-15 km towards the contact with the granite (Greenfield et al., 1996; Greenfield, Clarke, & White 1998; Vernon et al., 1990; White et al., 2003). The strong temperature increase cross the sequence (from ~500 °C in Zone 1 to ~820 °C in Zone 4) is accompanied by only a minor increase in pressure from ~3 to ~4 kbar (Figure 1b; Greenfield et al., 1996; Vernon et al., 1990; White et al., 2003).

Prograde metamorphism and anatexis occurred between *c.* 1795 and *c.* 1805 Ma and were synchronous with granite emplacement (*c.* 1802 Ma; Rubatto, Hermann, & Buick, 2006). Granite truncates the metamorphic isograd pattern (Clarke, Collins, & Vernon 1990; Greenfield et al., 1996) and contains xenoliths of the metamorphic country rocks (Collins & Williams, 1995). For these reasons, the low-*P* high-*T* metamorphism is considered to be due

to a combination of a local and regional heat source (Greenfield et al., 1996; Rubatto et al., 2006).

3.2.1 Mt. Stafford metapelitic migmatites

This contribution is focused on migmatites of a pelitic composition. The reader may refer to Greenfield et al. (1996, 1998), Palya, Buick, and Bebout (2011), Vernon et al. (1990), Wang, Dunkley, Clarke, and Dazko (2014) and White et al. (2003) for a detailed petrographic description of rocks across the sequence. Zone 1 is characterized by low-grade muscovite-quartz schists. Tourmaline may be an accessory mineral. Within Zone 2, Zone 2a is defined by the subsolidus breakdown of muscovite to andalusite and K-feldspar, whereas the Zone 2a-2b boundary marks the onset of partial melting (Figure 1b). Here rocks are characterized by thin interconnected leucosomes oriented predominantly normal to bedding; they are inferred to reflect the onset of H₂O-present melting (Greenfield et al., 1996). The occurrence of tourmaline and, in turn, of boron likely lowered the wet solidus in some rocks (Figure 1b; Greenfield et al., 1996, 1998; White et al., 2003). The boundary between Zones 2b and 2c is defined by the appearance of sillimanite often pseudomorphing andalusite. In Zone 3 (720–760 °C) biotite mode strongly decreases and migmatites show well-developed melanosome. Schlieren diatexites are also described. Zone 4 contains numerous diatexites and metapsammitic rocks are characterized by the appearance of orthopyroxene. In contrast, Zone 5 consists of biotite-rich hybrid diatexites that contain both internally-derived partial melts and injected granitic veins (Greenfield et al., 1996, 1998). Zone 5 appears to record lower-grade metamorphic conditions than Zone 4 (Greenfield et al., 1998; Vernon et al., 1990).

High-grade rocks show a somewhat large compositional heterogeneity and different Bt-bearing and Bt-absent granulite-facies assemblages have been documented in metapelites from Zone 4, such as Crd–Spl–Kfs–Qtz, Crd–Spl–Kfs–Sil, Crd–Spl–Kfs–Qtz–Sil, Crd–Spl–Grt–Kfs–Qtz, Bt–Grt–Crd–Sil–Pl–Kfs–Ilm–Qtz, Bt–Crd–Sil–Pl–Kfs–Ilm, Grt–Crd–Pl–Kfs–Ilm–Qtz and Crd–Sil–Pl–Kfs–Ilm–Qtz–Mt (e.g., Greenfield et al., 1996; Palya et al., 2011; Wang et al. 2014; White et al. 2003). K-feldspar and cordierite are often the most abundant minerals in Zone 4 rocks and may comprise over 80% of the assemblage in a sample (e.g., Palya et al., 2011).

Anatectic melt in Zones 3 and 4 was mainly produced by a series of multivariant biotite breakdown reactions experienced by the different rock types (White et al., 2003). Rocks from Zone 4 are expected to have had ~20–25 wt.% melt at peak conditions (Wang et al., 2014; White et al., 2003). Melting was contemporaneous with localized extension, as indicated by segregation of melt into cm- to dm-scale boudin necks and conjugate shear zones (Greenfield et al., 1996, 1998; White et al., 2003). Melt loss is documented by depletion in Si, K, Cs, Rb, U, B, Li of some samples from Zone 4 with respect to the protolith compositions (Palya et al., 2011).

4 PHASE EQUILIBRIA MODELLING

One of the best characterized Bt–Grt–Sil enclaves from El Hoyazo (sample HO50) and a residual metapelitic migmatite from Zone 4 at Mt. Stafford (sample MST45) have been selected for modelling. Enclave HO50 shows a very residual composition (SiO₂ ~45 wt.%, Al₂O₃ ~30 wt.%, FeO ~13 wt.%). On the other hand, the Mt. Stafford migmatite MST45 is chosen because, despite the clear chemical evidence of melt loss with respect to Zone 1 protoliths (FeO ~8 wt.%, Rb ~200 ppm, Cs ~4 ppm, U ~4 ppm; see Palya et al., 2011), the residual character of this rock is not extreme (SiO₂ ~55 wt.%).

Phase diagrams have been constructed using the *Perple_X* software (Connolly, 2009) with the thermodynamic database of Holland & Powell (1998, as revised in 2003). Two different model chemical systems $\text{Na}_2\text{O}-\text{CaO}-\text{K}_2\text{O}-\text{FeO}-\text{MgO}-\text{Al}_2\text{O}_3-\text{SiO}_2-\text{H}_2\text{O}-\text{TiO}_2$ (NCKFMASHT) and $\text{Na}_2\text{O}-\text{CaO}-\text{K}_2\text{O}-\text{FeO}-\text{MgO}-\text{Al}_2\text{O}_3-\text{SiO}_2-\text{H}_2\text{O}$ (NCKFMASH) were selected. The Ti component plays a fundamental role in extending the stability field of biotite in P - T space (Tajčmanová, Connolly, & Cesare, 2009; and references therein). On the other hand, the involvement of this component may produce an unrealistic decrease of modal proportions of some key Ti-free minerals (e.g., garnet, muscovite) at near-solidus conditions (Bartoli, Tajčmanová, Cesare, & Acosta-Vigil 2013; Bartoli, Acosta-Vigil, Tajčmanová, Cesare, & Bodnar, 2016b). Because muscovite melting seems to have played an important role in the anatectic history of El Hoyazo samples (Acosta-Vigil et al., 2010), near solidus calculations for granulite HO50 were done in the Ti-free system, whereas Ti was considered for the high-temperature phase equilibria to obtain more realistic estimates of the amounts of biotite consumed and melt produced. Conversely, muscovite breakdown commonly occurs in the subsolidus field at low- P conditions. It follows that phase diagrams of Mt. Stafford migmatite were all constructed in the Ti-bearing system.

Bt-Grt-Sil enclaves from El Hoyazo contain graphite, implying the involvement of a graphite-saturated COH fluid, as confirmed by the presence of primary CO_2 -bearing fluid inclusions (Cesare et al., 2007; Ferrero, Bodnar, Cesare, & Viti, 2011). In such a system, the H_2O activity is lowered below unity due to the presence of diluting carbonic species such as CH_4 and/or CO_2 (Connolly & Cesare, 1993). The involvement of the C component in the construction of pseudosections for anatectic rocks is a recent advance (e.g., Chu & Ague, 2013). In particular, it has been demonstrated that the decrease of $a_{\text{H}_2\text{O}}$ has a significant impact on the position of the fluid-saturated solidus at low- P conditions (<4-5 kbar; Bartoli et al., 2016b; Chu & Ague, 2013). For example, in graphite-bearing metagreywackes studied by Bartoli et al. (2016b) the shift of the solidus from C-bearing to C-absent systems is $\sim 100^\circ\text{C}$ at 2 kbar. Because the C quantification in MI is still in progress, the minimum shift of the fluid-saturated solidus is expected to be negligible at the pressures of 6 kbar (cf. Bartoli et al., 2016b; Cesare, Marchesi, Hermann, & Gomez-Pugnaire, 2003; Chu & Ague, 2013) and the melt model used does not account for the solubility of carbonic species, C component was not considered in the phase equilibria modelling performed in this study. The solution models used are: melt from White, Powell, and Holland (2007), garnet from Holland & Powell (1998), biotite from Tajčmanová et al. (2009), white mica from Coggon and Holland (2002), plagioclase from Newton, Charlu, and Kleppa (1980) and K-feldspar from Thompson and Hovis (1979). An ideal model was used for cordierite and ilmenite.

4.1 Phase equilibria modelling using the residuum composition

A first series of P - T pseudosections was calculated using the estimated bulk compositions (data from Palya et al., 2011 and Tajčmanová et al., 2009). The amount of H_2O in the bulk compositions was modified so that the observed peak assemblages are stable just above the solidus to reflect the conditions where these assemblages are in equilibrium with the last remaining melt after last melt loss event (see Diener et al., 2008, 2013; Korhonen et al., 2010; White et al., 2004; Yakymchuk et al., 2015). Moreover, this procedure can remove the possible effects of later subsolidus retrogression (White et al., 2004). H_2O values of 0.39 and 0.50 wt.% were determined for samples HO50 and MST45 using the T - H_2O diagrams calculated at 6 and 3.8 kbar (Figure 2a,b), and the corresponding P - T pseudosections are shown in Figure 2c,d (bulk composition reported in Table 1). These diagrams are only valid for assessing the peak and retrograde evolution of granulite HO50 and migmatite MST45, having been constructed using the composition of the residuum after anatexis and melt extraction (White et al., 2004).

In the case of the El Hoyazo sample, the inferred peak assemblage Grt–Bt–Sil–Pl–Ilm–Kfs–Liq (cf. table 1 in Acosta-Vigil et al., 2010) corresponds to a quadrivariant field in the high- T part of the diagram (Figure 2c). The low- T boundary of the Grt–Bt–Sil–Pl–Ilm–Kfs–Liq assemblage coincides with the solidus (Liquid-in curve). The relevant compositional isopleths of garnet ($X_{Alm}=0.80$, $X_{Grs}=0.03$), biotite ($X_{Mg}=0.35$; $Ti=0.30$ p.f.u.) and plagioclase ($X_{An}=0.33$) cross consistently in this quadrivariant field (Figure S2), indicating that sample HO50 equilibrated at 820–850 °C and 5.5–6.5 kbar (Figures 2c and S2), in agreement with previous estimates (Cesare et al., 1997; Tajčmanová et al., 2009). Biotite disappears at ~890 °C, whereas corundum appears at ~860 °C (Figure 2c).

Considering Mt. Stafford migmatite, the inferred peak assemblage Grt–Crđ–Pl–Kfs–Ilm–Qtz–Liq corresponds to a quadrivariant field in the high- T part of the diagram (Figure 2d). The low- T boundary coincides with the solidus and with the Bt-out curve at <3.5 kbar. Although the mineral chemistry of sample MST45 is not reported in the literature, cordierite and K-feldspar amounts are predicted to exceed 80 wt.% at the inferred peak conditions of 800–820 °C and 3.8–4.0 kbar (Figures 2d and S3) in agreement with natural observations (Palya et al., 2011).

The proportions of melt predicted by the modelling at 850 °C and 6 kbar (El Hoyazo) and at 810 °C and 4.0 kbar (Mt. Stafford) are <1–2 wt.% (Figures S2 and S3), significantly lower than the amount suggested by field observations, microstructures, geochemistry and mass balance calculations. This discrepancy is expected in the case of pseudosections constructed for residual (i.e., less fertile) compositions.

4.2 Melt-reintegration approach

The melt-reintegration approach consists of the addition of melt of a composition in equilibrium with the residuum at a given pressure and temperature (White et al., 2004). A second series of P – T pseudosections was constructed progressing step by step to lower temperatures along the inferred P – T paths of Figure 1. Pseudosection panels and modal abundance boxes for El Hoyazo and Mt. Stafford rocks are presented in Figures 3 and 4, and Figures 5 and 6, respectively.

In the case of the El Hoyazo enclave, calculations were initially performed reintegrating the measured MI and matrix glass compositions and considering the melt amounts inferred by mass-balance calculations (method 1). Subsequently and in the case of Mt. Stafford migmatites, reintegration has been done following the different single- and multi-step approaches proposed in the literature (methods 2, 3 and 4).

The bulk compositions used to calculate pseudosections are reported in Table 1, whereas those of reintegrated melts are in Table S1. Changes in bulk composition during melt-reintegration, as well as the final protolith compositions, can also be monitored in Figures 7 and 8.

4.2.1 Reintegrating measured melt compositions and calculated melt amounts (El Hoyazo sample)

Method 1. The investigated enclave HO50 experienced prograde melting from ~700 to ~850 °C and melt loss. Although the actual number of melt drainage events along the prograde path is not known, each melting reaction seems to have been able to produce an amount of melt higher than that required for melt escape, ~7 vol.% (~6 wt.%) corresponding to the melt connectivity transition (MCT) of Rosenberg and Handy (2005). Therefore, it is reasonable to assume that at least three different melt loss events occurred during prograde heating.

Considering the inferred prograde history and the trace element signatures of the analyzed melts (Figure 1a), the composition of the matrix glass was reintegrated at 825 °C, whereas that of MI in garnet and plagioclase at 770 and 720 °C, respectively. Because the enclaves still have melt present as primary MI and as films along foliation planes of the matrix (Cesare et al., 1997; Acosta-Vigil et al., 2007), the volume of melt to be reintegrated at each step cannot be that modelled for the main melting reactions (Figure 1a). According to the modal abundance of plagioclase, garnet and matrix glass in the enclave HO50 (see Acosta-Vigil et al., 2010) and considering the abundance of MI within host crystals (Acosta-Vigil et al., 2007), the amount of melt to reintegrate at each step in the modelling has been assumed to be 12 wt.% at 825 °C, 23 wt.% at 770 °C and 15 wt.% at 720 °C. This results in the cumulative reintegration of 50 wt.% melt, in accordance with estimates by Cesare et al. (1997). After each reintegration, the obtained bulk composition is then used to construct a new pseudosection and this new bulk composition is used for the next melt-reintegration step.

The resulting P - T pseudosection is shown in Figure 3a, where the solidus calculated with the observed residual composition is shown for reference. If compared with the pseudosection for the residuum (Figure 2c), the topology of Figure 3a is, predictably, significantly different. For the melt-reintegrated composition, the entire solidus is H_2O -saturated and it is located at lower temperature than that in the residual sample. In particular, the shift of the solidus towards lower temperatures is ~ 160 °C at the pressure of interest (6 kbar), and ~ 200 °C at ≤ 5 kbar (Figure 3a). Cordierite is stable only above the solidus at ≤ 5 kbar. Quartz disappears between 770 and 800 °C. The M_s -out curve coincides with the H_2O -saturated solidus between 4 and 5 kbar, whereas at 6 kbar muscovite is totally consumed in the soprasolidus at ~ 700 °C (Figures 3a and 4a). Biotite abundance decreases with increasing temperature and it is around 10 wt.% at ~ 850 °C, ~ 6 kbar (Figure 4a).

4.2.2 Reintegrating calculated melt compositions and arbitrary melt amounts (El Hoyazo and Mt. Stafford samples)

Single-step method 2. Figures 3b and 5a show the P - T pseudosections for the samples HO50 and MST45 obtained by reintegrating in one step the melt calculated at the intersection of the residuum solidus for the residual compositions with the inferred P - T paths, i.e., at 825 °C and 6 kbar (El Hoyazo) and at 800 °C and 3.7 kbar (Mt. Stafford). The minimum amounts of reintegrated melt to saturate the solidus in H_2O at the pressures of interest are 27 and 24 wt.%, respectively (Figures 3b and 5a).

For enclave HO50, quartz is predicted to be stable up to ~ 700 °C and biotite up to ~ 770 °C (at 6 kbar), respectively (Figures 3b and 4b). The disappearance of biotite before reaching peak conditions is not consistent with petrographic and geochemical observations and is related to the chosen Ti-free chemical system (Figure 3b). If Ti is considered in near-solidus calculations, biotite is stabilized up to ~ 900 °C and quartz disappears at ~ 800 °C, but muscovite is entirely consumed in the subsolidus at < 7.5 kbar and is not involved in the melting process (not shown). The latter is in contrast to the geochemical signature of MI in plagioclase and garnet (Acosta-Vigil et al., 2010). These observations highlight the importance of the choice of the appropriate model chemical system in reproducing natural rocks by means of phase equilibria modelling, because the obtained results can be misleading (see discussion in White et al., 2007). Despite the chosen chemical system, 21-24 wt.% of melt is predicted to be produced along the El Hoyazo prograde path before the melt loss event at 825 °C (Figure 4b).

Considering Mt. Stafford migmatite MST45, muscovite disappears before reaching the H₂O-saturated solidus and melting starts at ~660 °C and ~3.1 kbar (Figures 5a and 6a). Biotite is predicted to be stable up to ~790 °C (Figure 6a).

Multi-step method 3. Following the original method proposed by White et al. (2004), a total of 15 wt.% melt was added back to sample HO50 in six reintegration steps along the inferred isobaric P - T path at 825, 805, 794, 763, 707 and 700 °C, and 6 kbar (Figure 3c). The H₂O-saturated solidus was encountered at 670 °C (at 6 kbar). Similarly, five reintegration steps (at 800, 795, 782, 725 and 720 °C) are needed to generate a H₂O-saturated solidus at ~660 °C and ~3.2 kbar for migmatite MST45 after adding back 18 wt.% melt (Figure 5b). The topology of pseudosections (Figures 3c and 5b) and mode amounts (Figures 4c and 6b) are comparable with those of diagrams for method 2.

Multi-step method 4. Following the method originally proposed by Korhonen et al. (2013), a H₂O-saturated solidus was obtained at ~675 °C (6 kbar) and at ~660 °C (3.1 kbar), respectively, after reintegration of a total of 20 wt.% melt in four steps (Figures 3d and 5c). The resulting P - T pseudosections and mode amounts are similar to those previously obtained (Figures 3-6).

5 DISCUSSION

5.1 Model protolith composition

5.1.1 El Hoyazo granulitic enclaves

The final model protolith composition HO50f obtained by reintegrating measured melt compositions and calculated melt amounts (method 1), plots inside the compositional field of metasedimentary rocks from the Alboran Sea basement and the nearby Alpujarride complex (Figure 7). These rocks are considered to be the analogous of the source rocks of NVP melts (Cesare et al., 1997). Although the link between the residual enclaves and their protolith is not explicit and the chemical variability of basement rocks is broad (Figure 7), the reintegrated composition HO50f might represent an acceptable protolith composition of El Hoyazo enclaves. Methods 2, 3 and 4, instead, resulted in protolith compositions (HO50g, HO50m and HO50q; Table 1) more residual –i.e., showing higher FeO, MgO, Al₂O₃, CaO and TiO₂ and lower SiO₂, K₂O and H₂O with respect to the expected protolith composition (Figure 7). For example, FeO and MgO are up to 29 and 43 % relatively more enriched, whereas K₂O and H₂O are moderately to highly depleted (up to -16 and -47 % relative compared with protolith composition HO50f).

It could be correctly argued that knowing exactly the protolith composition is essential for evaluating the various methods. However, the fact that similar results have been also found for a highly residual migmatite from Mt. Stafford area –for which protolith composition is, instead, precisely constrained (see discussion below)– allows one to be more confident about the inferences reported above.

5.1.2 Mt. Stafford migmatite

The model protolith compositions MST45a, MST45f and MST45j obtained by applying melt-reintegration approaches from the literature (methods 2, 3 and 4) plot inside the compositional field of unmelted rocks from Zones 1 and 2a (Figure 8). Therefore, all the applied methods seem to provide acceptable protolith compositions.

5.2 Melting conditions and reactions inferred by melt-reintegration approach

5.2.1 El Hoyazo granulitic enclaves

For the melt-reintegrated composition HO50f obtained from method 1, the solidus is at lower temperature than that in the residual sample (compare Figures 2c and 3a), as expected for a fertile metasedimentary rock. According to the melt-reintegrated P – T pseudosection and assuming the isobaric P – T path previously proposed for this section of continental crust, melting begins at the H_2O -saturated solidus at ~ 660 °C, 6 kbar consuming muscovite, and evolves towards a fluid-absent state in which further melting proceeded by H_2O -undersaturated melting of muscovite and then biotite (Figures 3a and 4a). Quartz disappears at ~ 800 °C, just before reaching peak conditions. This likely inhibited further extensive melting and favoured the persistence of biotite at 800–850 °C (Cesare, 2000; Cesare et al., 1997). Corundum is predicted to be stable at >860 °C (for Ti-bearing system) and its absence in this and other enclaves is consistent with a maximum peak conditions of ~ 850 °C (Figure 3a). At peak temperatures, cordierite appears at < 5 kbar, reinforcing the inference that its growth mainly occurred during a decompression event after reaching peak conditions (Álvarez-Valero et al. 2007). This is in accordance with microstructural observations of sample HO50 suggesting that cordierite formed after the development of the foliation defined by peak mineral assemblage (Acosta-Vigil et al., 2010).

Similar melting conditions and reactions can be inferred from the various phase diagrams obtained applying melt-reintegration approaches from the literature (Figure 3b-d). Some discrepancies in phase modes (Figure 4) mostly depend on the selected chemical system –i.e., Ti-bearing or -absent (see discussion above).

Some degrees of reaction overstepping are expected in these rocks characterized by rapid heating (Cesare & Maineri, 1999). This can explain the apparent decoupling between phase equilibria modelling, which predicts the presence of garnet and plagioclase from subsolidus conditions (Figure 4), and the occurrence of MI in crystal cores (Figure S2b,c) which, instead, prove their crystallization in the presence of melt (i.e., beyond the solidus; see discussion in Cesare & Maineri, 1999; Cesare et al., 2015). Taking into account i) that equilibrium-based models are simplified proxies for natural systems (White et al., 2011), ii) that important minor components such as Mn and Fe^{3+} are not considered, and iii) that important departures from rock-wide equilibrium may occur during reactions (Carlson, Pattison, & Caddick, 2016), the prograde history inferred by melt-reintegration approach can be considered satisfactory because it considerably matches that inferred by microstructures, geochemistry and mass-balances.

5.2.2 Mount Stafford migmatites

According to the melt-reintegrated P – T pseudosections and assuming the proposed P – T path (Figure 1b), muscovite disappears in the subsolidus field and the H_2O -saturated solidus is encountered at ~ 650 °C and 3.1 kbar. Quartz, sillimanite and biotite amounts decrease rapidly with rising temperature and melt is mainly produced in the absence of an aqueous fluid phase by biotite-consuming reactions (Figure 5). Cordierite and K-feldspar are the common peritectic phases (Figure 6). Biotite mode strongly decreases up to ~ 720 °C, in correspondence of the low- T boundary of Zone 3 (Figure 6), as suggested by White et al. (2003). Biotite is totally consumed before reaching the thermal peak (Figure 5), and the rock is dominated by cordierite, K-feldspar and melt with minor amounts of garnet, plagioclase and ilmenite at peak conditions (Figure 6). The described prograde history is in agreement with that reconstructed by previous studies (see above).

On the basis of pseudosections of Figure 5, melting of Mt. Stafford rocks occurs in the sillimanite field. However, andalusite has been documented in Zone 2c (i.e. beyond the solidus) where it is pseudomorphosed by sillimanite (Greenfield et al., 1996; Vernon et al., 1990). This discrepancy between petrographic evidence and phase equilibria modelling can be explained by the metastable persistence of andalusite within the sillimanite field. This occurrence has been already documented in other metamorphic terranes and a detailed discussion about this topic is presented in White et al. (2003) for Mt. Stafford migmatites.

5.3 Estimates of melt productivity of crustal rocks

Accurately assessing the melt productivity of crustal rocks is essential to explore the potential role of melt loss and redistribution in the evolution of the continental crust. Pervasive migration and redistribution of melt may produce felsic injection complexes, and has several broad implications for the continental crust such as the rehydration of adjacent rocks and the increase of radiogenic heat production (see Berger, Burri, Alt-Epping, & Engi, 2008; Korhonen et al., 2013; Morfin, Sawyer, & Bandyayera, 2013; Morfin et al., 2014). Moreover, accumulation of melt causes a weakening of the injected structures and a decrease of their density. Yakymchuk & Brown (2014a) demonstrated that when a subsolidus metapelitic crust accommodates 50 vol.% melt it becomes ~10% less dense. These authors argued that such a decrease of density may have a significant impact on the development of detachments, migmatitic domes and metamorphic core complexes (see Yakymchuk & Brown, 2014a).

Estimates of the amount of melt produced during crustal anatexis have been obtained by melting experiments (Clemens, 2006, and references therein), geochemical mass balance methods (Carvalho et al., 2016; Guernina & Sawyer, 2003) and phase equilibria calculations (Webb, Powell, & McLaren, 2015; White, Powell, & Holland, 2001; Yakymchuk et al., 2013). A common approach consists in considering the probable melt productivity of the model protolith composition reconstructed by melt-reintegration approach (e.g., Cai et al., 2014; Diener et al. 2014; Guilmette et al., 2011; Hasalová et al., 2008; Indares et al., 2008; Nicoli et al., 2015; Taylor et al., 2014; White et al., 2004; Zhang et al., 2015). These amounts of melt are a maximum, because melt loss would reduce rock fertility at higher temperature (Korhonen et al., 2010; Yakymchuk & Brown, 2014b). However, the relative melt productivity among different protoliths remains representative, as suggested by Diener et al. (2014).

5.3.1 El Hoyazo granulitic enclaves

Protolith composition HO50f, obtained by reintegrating measured melt compositions and calculated melt amounts (method 1), would produce ~16-22, ~24-33 and ~48-50 wt.% melt at 700, 750 and 850 °C (6 kbar) respectively, and considering Ti-bearing and Ti-free chemical systems (Figure 9a). At the same reference temperatures, the more residual compositions HO50g, HO50m and HO50q (obtained from methods 2, 3 and 4) show much smaller melt amounts: ~5-9, ~7-15 and ~20-28 wt.% (Figure 9a). A maximum melt productivity of ~50 wt.% at peak conditions is consistent with the petrogenetic history of these rocks (Acosta-Vigil et al., 2011; Cesare et al., 1997). If the bulk composition obtained by reintegrating melt inclusion compositions is assumed to be representative of the actual protolith composition, then the other methods underestimate melt productivity by up to ~90% at low-temperature (~700 °C), and 45-60 % at 850 °C (Figure 9a).

5.3.2 Mount Stafford migmatites

The three model protolith compositions (MST45a, MST45f and MST45j) obtained by methods 2, 3 and 4 would produce similar melt amounts: 4-6, 8-10 and 18-21 wt.% melt at 700, 750 and 800 °C, respectively (Figure 9b). A maximum melt productivity of 22-23 wt.% is predicted at peak temperature of 820 °C (Figure 9b), in agreement with previous estimates (White et al., 2003).

In contrast to El Hoyazo samples, the precise protolith compositions are well known at Mt. Stafford area. Notably, White et al. (2003) performed forward phase equilibria modelling of Zone 1 metapelites 1107Pe and 9115Pe to reconstruct the anatectic history of Mt. Stafford metapelitic migmatites. Two P - T pseudosections have been constructed considering the bulk composition of these un-melted rocks (Figure S4). Prograde melting along the proposed P - T path would produce 4-5, 8-10, 15-16 and 18-26 wt % melt at 700, 750, 800 and 820 °C, respectively (Figure 9b). Therefore, melt-reintegration approaches applied in this study led to model protolith compositions whose estimates of melt productivity at peak conditions match those expected for Mt. Stafford migmatites (Figure 9b).

5.4 An evaluation of the melt-reintegration approach

Being the suprasolidus crust anisotropic and a highly dynamic nonlinear system (Brown, 2007), it is clear that a wide variety of melt extraction scenarios is possible. Therefore, the real melt loss history in anatectic terranes remains mostly obscured and impossible to retrieve. Despite this degree of uncertainty, the different melt-reintegration approaches tested in this work produce similar phase diagrams in terms of first-order topology (Figures 3-6). These similarities confirm the outcome of previous forward modelling studies that different melt loss scenarios do not significantly change the major suprasolidus topologies of P - T pseudosections because they are largely controlled by solid phases (see Powell, Guiraud, & White, 2005; White & Powell 2002). This conclusion was used to argue that reintegrating a certain amount of melt into the measured residual composition is sufficient to recover an approximate protolith composition and, in turn, to investigate the prograde evolution (e.g., Guilmette et al., 2011; Indares et al., 2008; Lasalle & Indares, 2014; Palin et al., 2013). Indeed, similar prograde histories (in terms of melting conditions and reactions) can be inferred in spite of the different methods adopted and they match field, petrographic and geochemical evidence (see above). In addition, the calculated melt productivity for Mt. Stafford migmatites fits well with that determined by previous studies (Figure 9b).

However, the modelling performed on the El Hoyazo enclave demonstrates that, regardless of the different methods adopted, the development of a H_2O -saturated solidus at <700 °C after melt-reintegration cannot always be used as a reliable criterion to determine the amount of melt to be added back, because it does not guarantee the restoration of a reliable protolith composition (Figure 7). In the case of El Hoyazo granulites, this constraint seems to result in an underestimation of the amount of melt to be reintegrated (Figure 7). The reduction in bulk H_2O and K_2O diminishes the amount of total mica and water and hence melt productivity (Figure 9a).

An argument can be made that the discrepancy in melt productivity exhibited by the El Hoyazo enclaves should be smaller in the more common situation of slow heating. This is because the rapid heating, such as in the case of crustal melting triggered by mafic magma, may favour fluid retention from the low-grade protolith maximizing melt productivity (Acosta-Vigil et al., 2010; Buick, Stevens, & Gibson, 2004; Johnson, Brown, & White, 2010). Therefore, the wet solidus constraint (i.e., adding back an amount of melt until the

appearance of a H₂O-saturated solidus at <700 °C and at pressure of interest) does not work in this particular geological scenario.

On the other hand, the El Hoyazo granulitic enclaves are highly residual rocks (SiO₂ ~45 wt.%). In order to test if such a compositional feature may somehow affect the feasibility of the melt-reintegration approach, method 2 has been applied to a more residual migmatite from Mt. Stafford Zone 4 (sample MST16), characterized by 50 wt.% SiO₂, 30 wt.% Al₂O₃ and 12 wt.% FeO+MgO (Table 1). The Bt–Crd–Sil–Pl–Kfs–Ilm–Liq assemblage is predicted to be stable at peak conditions of 820 °C and 3.8 kbar (Figure S5). The development of a H₂O-saturated solidus at the pressure of interest (Figure S5) results in a model protolith composition which does not plot inside the compositional field of Zones 1 and 2b rocks –i.e. composition MST16a does not match the real protolith compositions of Mt. Stafford migmatites (Figure 8). A consequence of the underestimation of the melt to be reintegrated is that the predicted rock fertility of model protolith is reduced with respect to that expected (Figure 9b). In particular, the maximum melt content (12 wt.%) predicted at peak temperature for the model protolith of sample MST16 underestimates the expected values of 30-55 % (Figure 9b).

There are some robust examples in the literature in which the development of a H₂O-saturated solidus at <700 °C after melt-reintegration resulted in reliable model protolith compositions, and reliable prograde history inferences and rock fertility estimates. For instance, Redler, White, and Johnson (2013) investigated anatexis and melt loss processes in the crustal sequence of the Ivrea Zone (NW Italy). There, metapelites underwent partial melting from amphibolite- to granulite-facies conditions, with granulites showing significant melt loss prior to cooling. In order to model the prograde history of high-grade, melt-depleted rocks, these authors progressively reintegrated melt back into residual compositions until the wet solidus was reached. Fortunately, in the Ivrea Zone appropriate protoliths for granulites are present as amphibolite-facies metatexites, and a comparison between the two different types of modelling can be made. Both the melt-reintegrated pseudosections and those for amphibolite-facies rocks show a similar topology and melt productivity (see Redler et al. 2013).

Similarly, Yakymchuck et al. (2015) applied the melt-reintegration approach on migmatitic gneisses from West Antarctica, until the wet solidus was encountered at ~660 °C. Following this procedure, the reintegrated compositions exactly evolved towards the compositional field of the expected protoliths (cf. figure 4 in Yakymchuck et al., 2015). The fact that both Redler et al. (2013) and Yakymchuck et al. (2015) adopted the multi-step method initially proposed by White et al. (2004) (method 3 in this study) for bulk rock compositions in which the residual character is not extreme (SiO₂ >55 wt.%) supports the results of this study.

It is important to note that the reintegrated amount of melt –necessary to reconstruct a plausible protolith composition– may not reflect precisely the amount of melt lost along the prograde path. Indeed, multi-step approaches (in particular method 3) entail the reintegration of low-temperature, H₂O-rich melts (Figures 3 and 5; Table S1). Conversely, in the one-step reintegration method the melt composition is generally calculated at the intersection of the residuum solidus with the presumed prograde *P–T* path or at peak conditions (Figures 3b and 5a). Therefore, only a hotter and drier melt is generally added back and, in turn, a higher amount of melt is needed to obtain a H₂O-saturated solidus at the same *P–T* conditions, with respect to multi-step procedures (Figures 3 and 5).

Among proposed methods, method 4 (Korhonen et al., 2013) seems to be the most realistic from the geological point of view, because it is based on the 7 vol.% melt threshold of Rosenberg and Handy (2005). It is generally accepted that the attainment of this value should facilitate the development of a melt extraction network. However, deformation and associated pressure gradients are likely to lead to a critical threshold that is significantly lower than 7 vol.% (Brown, 2010b). Therefore, in the presence of syn-anatectic deformation, the method originally proposed by Korhonen et al. (2013) can be modified in order to add back a minor amount of melt (< 6 vol.%) for each reintegration step –i.e., melt-reintegration steps can be more closely spaced.

6 CONCLUSIONS

From the phase equilibria modelling performed in this study it can be concluded that:

- the single- and multi-step melt-reintegration approaches proposed in the literature provide comparable results;
- reintegrating melt into residual migmatites and granulites until the appearance of a H₂O-saturated solidus at <700 °C permits, in spite of the different methods adopted, reliable constraints on melting conditions and reactions, and on melt productivity to be obtained;
- the development of a H₂O-saturated solidus after melt-reintegration may not guarantee the restoration of a reliable protolith composition for highly residual (SiO₂ < 55 wt.%) migmatites and granulites or for rocks for which H₂O retention from subsolidus conditions is high. While melting conditions and reactions are likely to be successfully constrained, significant underestimations of melt productivity may occur and have to be taken into account when melt-reintegration approach is applied to these bulk compositions.

Overall, this comparative study confirms that reintegrating melt into residual compositions (White et al., 2004) is a reliable and useful approach to reconstruct a plausible prograde history for the melt-depleted suprasolidus crust by means of phase equilibria modelling.

ACKNOWLEDGEMENTS

The author is grateful to B. Cesare for providing the El Hoyazo sample and for critical reading of an earlier version of this manuscript, and to L. Tajčmanová for her helpful discussion on phase equilibria modelling. J.F.A. Diener and C. Yakymchuk are thanked for their thorough and insightful reviews that improved the quality of the manuscript. M. Brown is thanked for the very careful editorial handling. This research benefitted from funding from the Italian Ministry of Education, University, Research (Grant SIR RBSI14Y7PF to O.B.).

REFERENCES

- Abad, I., Nieto, F., Peacor, D.R., & Velilla, N. (2003). Prograde and retrograde diagenetic and metamorphic evolution in metapelitic rocks of Sierra Espuña (Spain). *Clay Minerals*, 38, 1–23.
- Acosta-Vigil, A., Barich, A., Bartoli, O., Garrido, C.J., Cesare, B., Remusat, L., Poli, S., & Raepsaet, C. (2016). The composition of nanogranitoids in migmatites overlaying the Ronda peridotites (Betic Cordillera, S Spain): the anatectic history of a polymetamorphic basement. *Contributions to Mineralogy and Petrology*, 171, 24.
- Acosta-Vigil, A., Buick, I., Cesare, B., London, D., & Morgan, G.B. VI (2012). The extent of equilibration between melt and residuum during regional anatexis and its implications for differentiation of the continental crust: a study of partially melted metapelitic enclaves. *Journal of Petrology*, 53, 1319–1356.
- Acosta-Vigil, A., Buick, I., Hermann, J., Cesare, B., Rubatto, D., London, D., & Morgan, G.B. VI (2010). Mechanisms of crustal anatexis: a geochemical study of partially melted metapelitic enclaves and host dacite, SE Spain. *Journal of Petrology*, 51, 785–821.

- Acosta-Vigil, A., Cesare, B., London, D., & Morgan, G.B. (2007). Microstructures and composition of melt inclusions in a crustal anatexic environment, represented by metapelitic enclaves within El Hoyazo dacites, SE Spain. *Chemical Geology*, *235*, 450–465.
- Acosta-Vigil, A., Pereira, M.D., Shaw, D.M., & London, D. (2001). Contrasting behaviour of boron during crustal anatexis. *Lithos*, *56*, 15–31.
- Álvarez-Valero, A. M., & Kriegsman, L. M. (2007). Crustal thinning and mafic underplating beneath the Neogene Volcanic Province (Betic Cordillera, SE Spain): evidence from crustal xenoliths. *Terra Nova*, *19*, 266–271.
- Álvarez-Valero, A., Cesare, B., & Kriegsman, L. M. (2007). Formation of spinel–cordierite–feldspar–glass coronas after garnet in metapelitic xenoliths: reaction modeling and geodynamic implications. *Journal of Metamorphic Geology*, *25*, 305–320.
- Álvarez-Valero, A., & Waters, D. J. (2010). Partially melted crustal xenoliths as a window into sub-volcanic processes: evidence from the Neogene Magmatic Province of the Betic Cordillera, SE Spain. *Journal of Petrology*, *51*, 973–991.
- Anderson, J. R., Kelsey, D. E., Hand, M., & Collins, W. J. (2013). Conductively driven, high-thermal gradient metamorphism in the Anmatjira Range, Arunta region, central Australia. *Journal of Metamorphic Geology*, *31*, 1003–1026.
- Bartoli, O., Acosta-Vigil, A., Ferrero, S., & Cesare, B. (2016a). Granitoid magmas preserved as melt inclusions in high-grade metamorphic rocks. *American Mineralogist*, *101*, 1543–1559.
- Bartoli, O., Acosta-Vigil, A., Tajčmanová, L., Cesare, B., & Bodnar, R.J. (2016b). Using nanogranitoids and phase equilibria modeling to unravel anatexis in the crustal footwall of the Ronda peridotites (Betic Cordillera, S Spain). *Lithos*, *256-257*, 282–99.
- Bartoli, O., Cesare, B., Remusat, L., Acosta-Vigil, A., & Poli, S. (2014). The H₂O content of granite embryos. *Earth and Planetary Science Letters*, *395*, 281–290.
- Bartoli, O., Tajčmanová, L., Cesare, B., & Acosta-Vigil, A., (2013). Phase equilibria constraints on melting of stromatic migmatites from Ronda (S. Spain): insights on the formation of peritectic garnet. *Journal of Metamorphic Geology*, *31*, 775–789.
- Benito, R., López-Ruiz, J., Cebriá, J. M., Hertogen, J., Doblas, M., Oyarzun, R., & Demaiffe, D. (1999). Sr and O isotope constraints on source and crustal contamination in the high-K calc-alkaline and shoshonitic Neogene volcanic rocks of SE Spain. *Lithos*, *46*, 773–802.
- Berger, A., Burri, T., Alt-Epping, P., & Engi, M. (2008). Tectonically controlled fluid flow and water-assisted melting in the middle crust: an example from the Central Alps. *Lithos*, *102*, 598–615.
- Boger, S. D., White, R. W., & Schulte, B. (2012). The importance of iron speciation (Fe⁺²/Fe⁺³) in determining mineral assemblages: an example from the high-grade aluminous metapelites of southeastern Madagascar. *Journal of Metamorphic Geology*, *30*, 997–1018.
- Bons, P.D., Druguet, E., Castaño, L.-M., & Elburg, M.A. (2008). Finding what is now not there anymore: Recognizing missing fluid and magma volumes. *Geology*, *36*, 851–854.
- Brown, M., 2001. Crustal melting and granite magmatism: key issues. *Physics and Chemistry of the Earth*, *26*, 201–212.
- Brown, M. (2007). Crustal melting and melt extraction, ascent and emplacement in orogens: mechanisms and consequences. *Journal of Geological Society, London*, *164*, 709–730.
- Brown, M. (2010). Melting of the continental crust during orogenesis: the thermal, rheological and compositional consequences of melt transport from lower to upper continental crust. *Canadian Journal of Earth Sciences*, *47*, 655–694.
- Brown, M. (2010b). The spatial and temporal patterning of the deep crust and implications for the process of melt extraction. *Philosophical Transactions of the Royal Society, Series A*, *368*, 11–51.
- Brown, M. (2013). Granite: from genesis to emplacement. *Geological Society of America*

Bulletin, 125, 1079–1113.

- Brown, C.R., Yakymchuk, C., Brown, M., Fanning, C.M., Korhonen, F.J., Piccoli, P.M., & Siddoway, C.S. (2016). From source to sink: petrogenesis of Cretaceous anatectic granites from Fosdick migmatite–granite complex, west Antarctica. *Journal of Petrology*, 57(7), 1241–1278.
- Buick, I. S., Stevens, G., & Gibson, R. L. (2004). The role of water retention in the anatexis of metapelites in the Bushveld Complex Aureole, South Africa: an experimental study. *Journal of Petrology*, 45, 1777–1797.
- Cai, J., Liu, F.L., Liu, P.H., Liu, C.H., Wang, F., & Shi, J.R. (2014). Metamorphic *P–T* path and tectonic implications of pelitic granulites from the Daqingshan Complex of the Khondalite Belt, North China Craton. *Precambrian Research*, 241, 161–184.
- Cai, J., Liu, F., Liu, P., Wang, F., Liu, C., & Shi, J. (2016). Anatexis record and *P–T* path evolution of metapelites from the Wulashan Complex, Khondalite Belt, North China Craton. *Precambrian Research*, <http://dx.doi.org/10.1016/j.precamres.2016.09.007>.
- Carlson, W., Pattison, D.R.M., & Caddick, M.J. (2016). Beyond the equilibrium paradigm: how consideration of kinetics enhances metamorphic interpretation. *American Mineralogist*, 100, 1659–1667.
- Carvalho, B.B., Sawyer, E.W., & Janasi, V.A. (2016). Crustal reworking in a shear zone: transformation of metagranite to migmatite. *Journal of Metamorphic Geology*, 34, 237–264.
- Cesare, B. (2000). Incongruent melting of biotite to spinel in a quartz-free restite at El Joyazo (SE Spain): textures and reaction characterization. *Contributions to Mineralogy and Petrology*, 139, 273–284.
- Cesare, B. (2008). Crustal melting: working with enclaves. In: Sawyer, E. W., & Brown, M. (eds) *Working with Migmatites*. Mineralogical Association of Canada, Short Course Series 38, 37–55.
- Cesare, B., Acosta-Vigil, A., Ferrero, S., & Bartoli, O. (2011). Melt inclusions in migmatites and granulites. In: Forster, M.A., & Fitz Gerald, J.D. (Eds.), *The Science of Microstructure—Part II*. Journal of Virtual Explorer. 38 (ISSN 1441–8142). (paper 2, Electronic edition).
- Cesare, B., Acosta-Vigil, A., Bartoli, O., & Ferrero, S. (2015). What can we learn from melt inclusions in migmatites and granulites? *Lithos*, 239, 186–216.
- Cesare, B., & Gómez-Pugnaire, M. T. (2001). Crustal melting in the Alborán domain: constraints from enclaves of the Neogene Volcanic Province. *Physics and Chemistry of the Earth*, 26, 255–260.
- Cesare, B., & Maineri, C. (1999). Fluid-present anatexis of metapelites at El Joyazo (SE Spain): constraints from Raman spectroscopy of graphite. *Contributions to Mineralogy and Petrology*, 135, 41–52.
- Cesare, B., Maineri, C., Baron Toaldo, A., Pedron, D., & Acosta-Vigil, A. (2007). Immiscibility between carbonic fluids and granitic melts during crustal anatexis: a fluid and melt inclusion study in the enclaves of the Neogene Volcanic Province of SE Spain. *Chemical Geology*, 237, 433–449.
- Cesare, B., Marchesi, C., Hermann, J., & Gomez-Pugnaire, M.T. (2003). Primary melt inclusions in andalusite from anatectic graphitic metapelites: implications for the position of the Al₂SiO₅ triple point. *Geology*, 31, 573–576.
- Cesare, B., Salvioli Mariani, E., & Venturelli, G. (1997). Crustal anatexis and melt extraction during deformation in the restitic xenoliths at El Joyazo (SE Spain). *Mineralogical Magazine*, 61, 15–27.
- Clarke, G. L., Collins, W. J., & Vernon, R. H. (1990). Successive overprinting granulite facies metamorphic events in the Anmatjira Range, central Australia. *Journal of Metamorphic Geology*, 8, 65–88.

- Clemens, J.D. (2006). Melting of the continental crust: fluid regimes, melting reactions and source-rock fertility. In: *Evolution and differentiation of the continental crust* (eds M. Brown, M., & T. Rushmer), p. 297–331. Cambridge University Press, U.K.
- Chen, Y., Ye, K., Liu, J.-B., & Sun, M. (2008). Quantitative P–T–X constraints on orthopyroxene-bearing high-pressure granulites in felsic–metapelitic rocks: evidence from the Huangtuling granulite, Dabieshan Orogen. *Journal of Metamorphic Geology*, *26*, 1–15.
- Chu, X., & Ague, J.J. (2013). Phase equilibria for graphitic metapelite including solution of CO₂ in melt and cordierite: implications for dehydration, partial melting and graphite precipitation. *Journal of Metamorphic Geology*, *31*, 843–862.
- Coggon, R., & Holland, T.J.B. (2002). Mixing properties of phengitic micas and revised garnet–phengite thermobarometers. *Journal of Metamorphic Geology*, *20*, 683–696.
- Collins, W. J., & Williams, I. S. (1995). SHRIMP ionprobe dating of short-lived Proterozoic tectonic cycles in the northern Arunta Inlier, central Australia. *Precambrian Research*, *71*, 69–89.
- Compston, D. M. (1995). Time constraints on the evolution of the Tennant Creek Block, northern Australia. *Precambrian Research*, *71*, 107–129.
- Connolly, J.A.D. (2009). The geodynamic equation of state: what and how. *Geochemistry, Geophysics, Geosystems*, *10*, Q10014.
- Connolly, J.A.D., & Cesare, B. (1993). C–O–H–S fluid composition and oxygen fugacity in graphitic metapelites. *Journal of Metamorphic Geology*, *11*, 379–388.
- Chen, Y., Ye, K., Liu, J.B., & Sun, M. (2008). Quantitative P–T–X constraints on orthopyroxene-bearing high-pressure granulites in felsic–metapelitic rocks: evidence from the Huangtuling granulite, Dabieshan Orogen. *Journal of Metamorphic Geology*, *26*, 1–15.
- Diener, J.F.A., & Fagereng, Å. (2014). The influence of melting and melt drainage on crustal rheology during orogenesis. *Journal of Geophysical Research: Solid Earth*, *119*, 6193–6210.
- Diener, J.F.A., White, R.W., & Hudson, T.J.M. (2014). Melt production, redistribution and accumulation in mid-crustal source rocks, with implications for crustal-scale melt transfer. *Lithos*, *200–201*, 212–225.
- Diener, J.F.A., White, R.W., Link, K., Dreyer, T.S., & Moodley, A. (2013). Clockwise, low-P metamorphism of the Aus granulite terrain, southern Namibia, during the Mesoproterozoic Namaqua Orogeny. *Precambrian Research*, *224*, 629–652.
- Diener, J.F.A., White, R.W., & Powell, R. (2008). Granulite facies metamorphism and subsolidus fluid-absent reworking, Strangways Range, Arunta Block, central Australia. *Journal of Metamorphic Geology*, *26*, 603–622.
- Dumond, G., Goncalves, P., Williams, M.L., & Jercinovic, M.J. (2015). Monazite as a monitor of melting, garnet growth and feldspar recrystallization in continental lower crust. *Journal of Metamorphic Geology*, *33*, 735–762.
- Ferrero, S., Bartoli, O., Cesare, B., Salvioli-Mariani, E., Acosta-Vigil, A., Cavallo, A., ... Battiston, S. (2012). Microstructures of melt inclusions in anatectic metasedimentary rocks. *Journal of Metamorphic Geology*, *30*, 303–322.
- Ferrero, S., Bodnar, R.J., Cesare, B., & Viti, C. (2011). Reequilibration of primary fluid inclusions in peritectic garnet from metapelitic enclaves, El Hoyazo, Spain. *Lithos*, *124*, 117–131.
- Fitzherbert, J.A. (2015). Refined peak and retrograde metamorphic isograds for the Broken Hill and Euriovie blocks, NSW. *Quarterly Notes*, *143* (1).
- García-Casco, A., & Torres-Roldán, R.F. (1999). Natural metastable reactions involving garnet, staurolite and cordierite: implications for petrogenetic grids and the extensional collapse of the Betic-Rif Belt. *Contributions to Mineralogy and Petrology*, *136*, 131–153.
- Greenfield, J. E. (1997). Migmatite formation at Mt Stafford, central Australia. Ph.D. thesis,

- University of Sydney, 231 pp.
- Greenfield, J. E., Clarke, G. L., Bland, M., & Clark, D. C. (1996). In-situ migmatite and hybrid diatexite at Mt Stafford, central Australia. *Journal of Metamorphic Geology*, *14*, 413–426.
- Greenfield, J. E., Clarke, G. L., & White, R. W. (1998). A sequence of partial melting reactions at Mt Stafford, central Australia. *Journal of Metamorphic Geology*, *16*, 363–378.
- Groppo, C., Rolfo, F., & Indares, A. (2012). Partial melting in the Higher Himalayan Crystallines of Eastern Nepal: the effect of decompression and implications for the “channel flow” model. *Journal of Petrology*, *53*, 1057–1088.
- Groppo, C., Rolfo, F., & Mosca, P. (2013). The cordierite-bearing anatectic rocks of the higher Himalayan crystallines (eastern Nepal): low-pressure anatexis, melt productivity, melt loss and the preservation of cordierite. *Journal of Metamorphic Geology*, *31*, 187–204.
- Groppo, C., Rubatto, D., Rolfo, F., & Lombardo, B. (2010). Early Oligocene partial melting in the Main Central Thrust Zone (Arun valley, eastern Nepal Himalaya). *Lithos*, *118*, 287–301.
- Guilmette, C., Indares, A., & Hébert, R. (2011). High-pressure anatectic metapelites from the Namche Barwa, Eastern Himalayan Syntaxis: textural evidence for partial melting, phase equilibria modelling and tectonic implications. *Lithos*, *124*, 66–81.
- Guernina, S., & Sawyer, E.W. (2003). Large-scale melt-depletion in granulite terranes: an example from the Archean Ashuanipi subprovince of Quebec. *Journal of Metamorphic Geology*, *21*, 181–201.
- Hallett, B.W., & Spear, F.S. (2014). The P – T history of anatectic pelites of the Northern East Humboldt Range, Nevada: evidence for tectonic loading, decompression, and anatexis. *Journal of Petrology*, *55*, 3–36.
- Handy, M.R., Mulch, A., Rosenau, M., & Rosenberg, C.L. (2001). A synthesis of the role of fault zones and melts as agents of weakening, hardening and differentiation of the continental crust. In: *The Nature and Tectonic Significance of Fault Zone Weakening*, (eds Holdsworth, R.E., Strachan, R.A., Magloughlin, J.F., & Knipe, R.J.), Vol. 186, pp. 305–332. Geological Society, London, Special Publication, London.
- Hasalová, P., Štípská, P., Powell, R., Schulmann, K., Janoušek, V., & Lexa, O. (2008). Transforming mylonitic metagranite by open-system interactions during melt flow. *Journal of Metamorphic Geology*, *26*, 55–80.
- Holland, T.J.B., & Powell, R. (1998). An internally consistent thermodynamic data set for phases of petrological interest. *Journal of Metamorphic Geology*, *16*, 309–343.
- Holland, T.J.B., & Powell, R. (2003). Activity-composition relations for phases in petrological calculations: an asymmetric multicomponent formulation. *Contributions to Mineralogy and Petrology*, *145*, 492–501.
- Jiang, Y.D., Štípská, P., Sun, M., Schulmann, K., Zhang, J., Wu, Q.H.,... Xiao, W.J. (2015). Juxtaposition of Barrovian and migmatite domains in the Chinese Altai: a result of crustal thickening followed by doming of partially molten lower crust. *Journal of Metamorphic Geology*, *33*, 45–70.
- Johnson, T.E., Brown, M., & White, R.W. (2010). Petrogenetic modelling of strongly residual metapelitic xenoliths within the southern Platreef, Bushveld Complex, South Africa. *Journal of Metamorphic Geology*, *28*, 269–291.
- Johnson, T.E., White, R.W. & Powell, R. (2008). Partial melting of metagreywacke: a calculated mineral equilibria study. *Journal of Metamorphic Geology*, *26*, 837–853.
- Kelsey, D.E., & Hand, M. (2014). On ultrahigh temperature crustal metamorphism: phase equilibria, trace element thermometry, bulk composition, heat sources, timescales and tectonic settings. *Geoscience Frontiers*, *6*, 311–356.
- Kohn, J.M. (2014). Himalayan metamorphism and its tectonic implications. *Annual Review of*

Earth and Planetary Sciences, 42, 381–419.

- Korhonen, F.J., Brown, M., Clark, C., & Bhattacharya, S. (2013). Osumilite-bearing equilibria and implications for the evolution of the Eastern Ghats Province, India. *Journal of Metamorphic Geology*, 31, 881–907.
- Korhonen, F.J., Saito, S., Brown, M., & Siddoway, C.S. (2010). Modeling multiple melt loss events in the evolution of an active continental margin. *Lithos*, 116, 230–248.
- Kretz, R. (1983). Symbols for rock-forming minerals. *American Mineralogist*, 68, 277–279.
- Indares, A., White, R.W., & Powell, R. (2008). Phase equilibria modelling of kyanite-bearing anatectic paragneiss from the central Grenville Province. *Journal of Metamorphic Geology*, 26, 815–836.
- Laporte D., Rapaille C., & Provost A. (1997). Wetting angles, equilibrium melt geometry, and the permeability threshold of partially molten crustal protoliths. In: *Granite: from segregation of melt to emplacement fabrics*. (eds Bouchez, J.L., Hutton D.H.W., & Stephens, W.E.). Kluwer Academic Publishers, Dordrecht, pp 31–54.
- Lasalle, S., & Indares, A. (2014). Anatectic record and contrasting P – T paths of aluminous gneisses from the central Grenville Province. *Journal of Metamorphic Geology*, 32, 627–646.
- Maaløe, S., & Scheie, A. (1982). The permeability controlled accumulation of primary magma. *Contributions to Mineralogy and Petrology*, 81, 350–357.
- McGee, B., Giles, D., Kelsey, E., & Collins, A.S. (2010). Protolith heterogeneity as a factor controlling the feedback between deformation, metamorphism and melting in a granulite-hosted gold deposit. *Journal of the Geological Society, London*, 167, 1089–1104.
- Miller, C.F., McDowell, S.M., & Mapes, R.W. (2003). Hot and cold granites? Implications of zircon saturation temperatures and preservation of inheritance. *Geology*, 31, 529–532.
- Morfin, S., Sawyer, E.W., & Bandyayera, D. (2013). Large volumes of anatectic melt retained in granulite facies migmatites: an injection complex in northern Quebec. *Lithos*, 168–169, 200–218.
- Morfin, S., Sawyer, E. W., & Bandyayera, D. (2014). The geochemical signature of a felsic injection complex in the continental crust: Opinaca Subprovince, Quebec. *Lithos*, 196–197, 339–355.
- Morrissey, L.J., Hand, M., Kelsey, D.E., & Wade, P.B. (2016a). Cambrian High-temperature Reworking of the Rayner–Eastern Ghats Terrane: Constraints from the Northern Prince Charles Mountains Region, East Antarctica. *Journal of Petrology*, 57, 53–92.
- Morrissey, L.J., Hand, M., Lane, K., Kelsey, D.E., & Dutch, R.A. (2016b). Upgrading iron-ore deposits by melt loss during granulite facies metamorphism. *Ore Geology Reviews*, 74, 101–121.
- Nahodilová, R., Faryad, S.W., Dolejš, D., Tropper, P., & Konzett, J. (2011). High-pressure partial melting and melt loss in felsic granulites in the Kutná Hora complex, Bohemian Massif (Czech Republic). *Lithos*, 125, 641–658.
- Newton, R.C., Charlu, T.V., & Kleppa, O.J. (1980). Thermochemistry of high structural state plagioclases. *Geochimica et Cosmochimica Acta*, 44, 933–941.
- Nicoli, G., Stevens, G., Moyen, & J.-F., & Frei, D. (2015). Rapid evolution from sediment to anatectic granulite in an Archean continental collision zone: the example of the Bandelierkop Formation metapelites, South Marginal Zone, Limpopo Belt, South Africa. *Journal of Metamorphic Geology*, 33, 177–202.
- Palin, R.M., Searle, M.P., Waters, D.J., Parrish, R.R., Roberts, N.M.W., Horstwood, M.S.A., ... Anh, T.T. (2013). A geochronological and petrological study of anatectic paragneiss and associated granite dykes from the Day Nui Con Voi metamorphic core complex, North Vietnam; constraints upon the timing of metamorphism within the Red River shear zone. *Journal of Metamorphic Geology*, 31, 359–387.

- Palin, R.M., Weller, O.M., Waters, D.J., & Dyck, B. (2016a). Quantifying geological uncertainty in metamorphic phase equilibria modelling; a Monte Carlo assessment and implications for tectonic interpretations. *Geoscience Frontiers*, 7, 591–607.
- Palin, R.M., White, R.W., Green, E.C.R., Diener, J.F.A., Powell R., & Holland, T.J.B. (2016b). High-grade metamorphism and partial melting of basic and intermediate rocks. *Journal of Metamorphic Geology*, 34, 871–892.
- Palya, A.P., Buick, I.S., & Bebout, G.E. (2011). Storage and mobility of nitrogen in the continental crust: Evidence from partially melted metasedimentary rocks, Mt. Stafford, Australia. *Chemical Geology*, 281, 211–226.
- Powell, R., Guiraud, M., & White, R. W. (2005). Truth and beauty in metamorphic phase-equilibria: conjugate variables and phase diagrams. *The Canadian Mineralogist*, 43, 21–33.
- Redler, C., White, R.W., & Johnson, T.E. (2013). Migmatites in the Ivrea Zone (NW Italy): Constraints on partial melting and melt loss in metasedimentary rocks from Val Strona di Omegna. *Lithos*, 175–176, 40–53.
- Rosenberg, C.L., & Handy, M.L. (2005). Experimental deformation of partial melted granite revisited: implications for the continental crust. *Journal of Metamorphic Geology*, 23, 19–28.
- Rubatto, D., Hermann, J., & Buick, I.S. (2006). Temperature and bulk composition control on the growth of monazite and zircon during low-pressure anatexis (Mount Stafford, Central Australia). *Journal of Petrology*, 47, 1973–1996.
- Ruiz-Cruz, M.D., & Sanz de Galdeano, C. (2014). Garnet variety and zircon ages in UHP metasedimentary rocks from the Jubrique zone (Alpujarride Complex, Betic Cordillera, Spain): evidence for a pre-Alpine emplacement of the Ronda peridotite. *International Geology Reviews*, 56, 845–868.
- Ruiz-Cruz, M.D., Sanz de Galdeano, C., & Lázaro, C. (2005). Metamorphic evolution of Triassic rocks from the transition zone between the Maláguide and Alpujarride complexes (Betic Cordilleras, Spain). *European Journal of Mineralogy*, 17, 81–91.
- Ruiz-Cruz, M.D., Franco, F., Sanz de Galdeano, C., & Novák, J. (2006). Evidence of contrasting low-grade metamorphic conditions from clay mineral assemblages in Triassic Alpujarride-Maláguide transitional units in the Betic Cordilleras, Spain. *Clay Minerals*, 41, 619–636.
- Sawyer, E. W. (1991). Disequilibrium melting and the rate of melt-residuum separation during migmatization of mafic rocks from the Grenville Front, Quebec. *Journal of Petrology*, 32, 701–738.
- Sawyer, E.W. (1994). Melt segregation in the continental crust. *Geology*, 22, 1019–1022.
- Sawyer, E.W. (2008). Atlas of Migmatites. The Canadian Mineralogist Special Publication 9. Mineralogical Association of Canada, Quebec; NRC Research Press, Ottawa.
- Sawyer, E. W., Cesare, B., & Brown, M. (2011). When the continental crust melts. *Elements*, 7, 229–234.
- Shrestha, S., Larson, K.P., Guilmette, C., & Smit, M.A. (2017). The *P-T-t* evolution of the exhumed Himalayan metamorphic core in the Likhu Khola region, East Central Nepal. *Journal of Metamorphic Geology*, DOI: 10.1111/jmg.12250
- Skrzypek, E., Štípská, P., A., & Cocherie A. (2012). The origin of zircon and the significance of U–Pb ages in high-grade metamorphic rocks: a case study from the Variscan orogenic root (Vosges Mountains, NE France). *Contributions to Mineralogy and Petrology*, 164, 935–957.
- Solar, G.S., & Brown, M. (2001). Petrogenesis of migmatites in Maine, USA: possible source of peraluminous leucogranite in plutons? *Journal of Petrology*, 42, 789–823.
- Spadea, P., & Prosser, G. (1999). Data report: major- and trace-element chemistry of Site 976 basement rocks (Alboran Sea). *Proceedings of the Ocean Drilling Program, Scientific*

Results, 161, 375–379.

- Stewart, A.J., Shaw, R.D., & Black, L.P. (1984). The Arunta Inlier: a complex ensialic mobile belt in central Australia. Part 1: stratigraphy, correlations and origin. *Australian Journal of Earth Sciences*, 31, 445–455.
- Štípská, P., Schulmann, K., & Powell, R. (2008). Contrasting metamorphic histories of lenses of high-pressure rocks and host migmatites with a flat orogenic fabric (Bohemian Massif, Czech Republic): a result of tectonic mixing within horizontal crustal flow? *Journal of Metamorphic Geology*, 26, 623–646.
- Tajčmanová, L., Conolly, J.A.D., & Cesare, B. (2009). A thermodynamic model for titanium and ferric iron solution in biotite. *Journal of Metamorphic Geology*, 27, 153–165.
- Taylor, J., Nicoli, G., Stevens, G., Frei, D., & Moyen, J.-F. (2014). The processes that control the leucosome composition in metasedimentary granulites: perspectives from the Southern Marginal Zone migmatites, Limpopo Belt, South Africa. *Journal of Metamorphic Geology*, 32, 713–742.
- Thompson, A.B., & Connolly, J.A.D. (1995). Melting of the continental crust: some thermal and petrological constraints on anatexis in continental collision zones and other tectonic settings. *Journal of Geophysical Research*, 100(B8), 15565–15579.
- Thompson, J.B., & Hovis, G.L. (1979). Entropy of mixing in sanidine. *American Mineralogist*, 64, 57–65.
- Tian, Z., Zhang, Z., & Dong, X. (2016). Metamorphism of high-pressure metagreywacke from the Eastern Himalayan Syntaxis: phase equilibria and P – T path. *Journal of Metamorphic Geology*, 34, 697–718.
- Tucker, N.M., Hand, M., Kelsey, D.E., & Dutch, R.A. (2015). A duality of timescales: Short-lived ultrahigh temperature metamorphism preserving a long-lived monazite growth history in the Grenvillian Musgrave–Albany–Fraser Orogen. *Precambrian Research*, 264, 204–234.
- Vernon, R. H., Clarke, G. L., & Collins, W. J. (1990). Local, mid-crustal granulite facies metamorphism and melting: an example in the Mount Stafford area, central Australia. In: *High Temperature Metamorphism and Crustal Anatexis* (eds Ashworth, J. R., & Brown, M.), pp. 272–319. London: Unwin Hyman.
- Vielzeuf, D., Clemens, J.D., Pin, C., & Moinet, E. (1990). Granites, granulites, and crustal differentiation. In: *Granulites and Crustal Evolution* (eds Vielzeuf, D., & Vidal, P.), Vol. 311, NATO ASI Series. pp. 59–86. Kluwer Academic Publications, Dordrecht.
- Vigneresse, J.-L., Barbey, P., & Cuney, M. (1996). Rheological transitions during partial melting and crystallization with application to felsic magma segregation and transfer: *Journal of Petrology*, 37, 1579–1600.
- Wang, D., & Guo, J. (2017). Late Archean high-pressure pelitic granulites in the Yinshan Block, North China Craton. *Precambrian Research*, <http://dx.doi.org/10.1016/j.precamres.2017.03.027>
- Wang, W.-RZ., Dunkley, E., Clarke, G.L., & Dazko, N.R. (2014). The evolution of zircon during low- P partial melting of metapelitic rocks: theoretical predictions and a case study from Mt Stafford, central Australia. *Journal of Metamorphic Geology*, 32, 791–808.
- Webb, G., Powell, R., & McLaren, S. (2015). Phase equilibria constraints on the melt fertility of crustal rocks: the effect of subsolidus water loss. *Journal of Metamorphic Geology*, 33, 147–165.
- White, R.W., Palin, R.M., & Green, E.C.R. (2017). High-grade metamorphism and partial melting in Archean composite grey gneiss complexes. *Journal of Metamorphic Geology*, 35, 181–195.
- White, R.W., & Powell, R. (2002). Melt loss and the preservation of granulite facies mineral assemblages. *Journal of Metamorphic Geology*, 20, 621–632.
- White, R.W., & Powell, R. (2010). Retrograde melt–residue interaction and the formation of

- near- anhydrous leucosomes in migmatites. *Journal of Metamorphic Geology*, 28, 579–597.
- White, R.W., Powell, R., & Clarke, G.L. (2003). Prograde Metamorphic assemblage evolution during partial melting of metasedimentary rocks at low pressures: migmatites from Mt Stafford, Central Australia. *Journal of Petrology*, 44, 1937–1960.
- White, R.W., Powell, R., & Halpin, J.A. (2004). Spatially-focussed melt formation in aluminous metapelites from Broken Hill, Australia. *Journal of Metamorphic Geology*, 22, 825–845.
- White, R.W., Powell, R., & Holland, T.J.B. (2001). Calculation of partial melting equilibria in the system $\text{Na}_2\text{O}-\text{CaO}-\text{K}_2\text{O}-\text{FeO}-\text{MgO}-\text{Al}_2\text{O}_3-\text{SiO}_2-\text{H}_2\text{O}$ (NCKFMASH). *Journal of Metamorphic Geology*, 19, 139–154.
- White, R.W., Powell, R., & Holland, T.J.B. (2007). Progress relating to calculation of partial melting equilibria for metapelites. *Journal of Metamorphic Geology*, 25, 511–527.
- White, R.W., Stevens, G., & Johnson, T.E. (2011). Is the crucible reproducible? Reconciling melting experiments with thermodynamic calculations. *Elements*, 7, 241–246.
- Yakymchuk, C., & Brown, M. (2014a). Consequences of open-system melting in tectonics. *Journal of the Geological Society*, 171, 21–40.
- Yakymchuk, C., & Brown, M. (2014b). Behaviour of zircon and monazite during crustal melting. *Journal of the Geological Society*, 171, 465–479.
- Yakymchuk, C., Brown, M., Clark, C., Korhonen, F.J., Piccoli, P.M., Siddoway, C.S., ... Vervoort, J.D. (2015). Decoding polyphase migmatites using geochronology and phase equilibria modeling. *Journal of Metamorphic Geology*, 33, 203–230.
- Yakymchuk, C., Brown, M., Ivanic, T.J., & Korhonen, F.J. (2013). Leucosome distribution in migmatitic paragneisses and orthogneisses: a record of self-organized melt migration and entrapment in a heterogeneous partially-molten crust. *Tectonophysics*, 603, 136–154.
- Yin, C., Zhao, G., Wei, C., Sun, M., Guo, J., & Zhou, X. (2014). Metamorphism and partial melting of high-pressure pelitic granulites from the Qianlishan Complex: Constraints on the tectonic evolution of the Khondalite Belt in the North China Craton. *Precambrian Research*, 242, 172–186.
- Zhang, Z., Xiang, H., Dong, X., Li, W., Ding, H., Gou, Z., & Tian, Z. (2015). Oligocene HP metamorphism and anatexis of the Higher Himalayan Crystalline Sequence in Yadong region, east-central Himalaya. *Gondwana Research*, 41, 173–187.
- Zeck, H.P. (1970). An erupted migmatite from Cerro del Hoyazo, SE Spain. *Contributions to Mineralogy and Petrology*, 26, 225–246.
- Zeck, H.P. (1992). Restite–melt and mafic–felsic magma mingling in an S-type dacite, Cerro del Hoyazo, southeastern Spain. *Transactions of the Royal Society of Edinburgh: Earth Sciences*, 83, 139–144.
- Zeck H.P., & Williams, I.S. (2002). Inherited and magmatic zircon from Neogene Hoyazo cordierite dacite, SE Spain–Anatectic source rock provenance and magmatic evolution. *Journal of Petrology*, 43, 1089–1104.
- Zeck H.P., Kristensen, A.B., & Williams, I.S. (1998). Post-collisional volcanism in a sinking slab setting—crustal anatectic origin of pyroxene-andesite magma, Caldear Volcanic Group, Neogene Alborán volcanic Province, southeastern Spain. *Lithos*, 45, 499–522.
- Zou, Y., Zhai, M., Santosh, M., Zhou, L., Zhao, L., Junsheng, L. & Shan, H., (2017). High-pressure pelitic granulites from the Jiao-Liao-Ji Belt, North China Craton: A complete P-T path and its tectonic implications. *Journal of Asian Earth Sciences*, 134, 103–121.

SUPPORTING INFORMATION

Additional Supporting Information may be found online in the supporting information tab for this article.

FIGURE CAPTIONS

Fig. 1. (a) Prograde history (redrawn after Acosta-Vigil et al., 2010) of melt formation in the continental crust beneath the Neogene Volcanic Province of SE Spain, recovered by studying crustal enclaves. A pressure of 6 kbar is suggested by independent estimates made by Cesare et al. (1997) and Álvarez-Valero & Waters (2010). The obtained zircon and monazite saturation temperatures (T_{Zrn} , T_{Mnz}) have to be considered as minimum estimates. Orange arrow: decompression path proposed by Álvarez-Valero et al. (2007). See Acosta-Vigil et al. (2010, 2012) for additional details. (b) Prograde history of Mt. Stafford rocks (drawn after Greenfield et al., 1996, 1998; Vernon et al., 1990; Wang et al., 2014; White et al., 2003). Boron-bearing wet granite solidus from Spicer et al. (2004).

Fig. 2. Phase equilibria modelling considering the bulk residual composition of the enclave HO50 (El Hoyazo) and migmatite MST45 (Mt. Stafford). Peak assemblage is underlined. Mineral abbreviations after Kretz (1983). (a, b) T - M_{H_2O} diagrams calculated at 6 and 3.8 kbar, in the NCKFMASHT chemical system, for determining the bulk H_2O content. The observed peak assemblages are stable just above the solidus for M_{H_2O} values ranging from 0.37 to 0.41 wt.% (a) and from 0.23 to 0.53 wt.% (b), respectively. Orange dashed lines: selected M_{H_2O} values. Owing to the very narrow range, an average M_{H_2O} value of 0.39 was chosen for El Hoyazo sample. A M_{H_2O} value of 0.50 was, instead, selected for Mt. Stafford migmatite because lower H_2O contents would result in the peak assemblage to be stable at unreasonably high temperature. Red lines: solidus. (c, d) P - T pseudosections calculated in the NCKFMASHT chemical system and using the bulk composition of the enclave HO50 and migmatite MST45 obtained from the T - M_{H_2O} diagram (see Table 1). Red line: solidus. Yellow ellipse: inferred P - T conditions of equilibration. See text for details.

Fig. 3. Melt-reintegration approach for granulitic enclave HO50 (El Hoyazo). Successive P - T pseudosection panels show from right to left the changes in the topology of the phase assemblage fields after each melt-reintegration step. The right-hand panel is always from the P - T pseudosection for the residuum composition. Labels reported above each panel refer to the bulk composition used for calculations (see Table 1) and the chosen chemical system (NCKFMASH or NCKFMASHT). Red continuous line: solidus. Red dotted line: solidus for the residuum composition. Yellow continuous line: muscovite-out curve. Blue continuous line: quartz-out curve. Orange continuous line: biotite-out curve. Green continuous line: cordierite-out curve. Light blue field: region where liquid H_2O is predicted. (a) P - T pseudosection obtained reintegrating compositions of melt inclusions and matrix glass (method 1). (b, c, d) P - T pseudosections derived from melt-reintegration methods proposed in the literature (methods 2, 3 and 4, respectively). Within the panel for bulk composition HO50j in figure (c), the phase assemblage change in absence of a melt-reintegration step (method 3) is due to a change of the chosen chemical system. 1) Bt–Ms–Pl–Grt–Qtz– H_2O –Liq; 2) Bt–Ms–Pl–Grt–Qtz–Liq; 3) Ms–Pl–Grt–Qtz–Liq; 4) Bt–Ms–Pl–Kfs–Sil–Grt–Qtz–Liq; 5) Bt–Ms–Pl–Sil–Grt–Qtz– H_2O –Liq; 6) Bt–Pl–Sil–Qtz– H_2O –Liq; 7) Bt–Pl–Grt–Sil–Qtz–Liq; 8) Bt–Pl–Kfs–Grt–Crd–Sil–Liq; 9) Pl–Kfs–Crd–Grt–Spl–Liq; 10) Pl–Kfs–Crd–Grt–Spl–Sil–Liq; 11) Ms–Pl–Grt–Sil–Qtz–Liq; 12) Ms–Pl–Kfs–Grt–Sil–Liq; 13) Bt–Ms–Pl–Kfs–Grt–Sil–Liq; 14) Ms–Pl–Kfs–Grt–Sil–Liq; 15) Bt–Pl–Grt–Ilm–Sil–Qtz–Liq; 16) Bt–Pl–

Kfs–Grt–Crd–Ilm–Spl–Liq; 17) Bt–Pl–Kfs–Grt–Crd–Ilm–Spl; 18) Bt–Pl–Kfs–Grt–Ilm–Sil–Spl–Liq; 19) Pl–Kfs–Grt–Crd–Ilm–Spl–Liq; 20) Bt–Pl–Grt–Crd–Sil–Qtz–H₂O; 21) Bt–Pl–Grt–Crd–Sil–Qtz–Liq; 22) Ms–Pl–Grt–Sil–Qtz; 23) Ms–Pl–Grt–Sil–Qtz–Liq; 24) Bt–Pl–Kfs–Crd–Grt–Spl–Liq; 25) Bt–Pl–Kfs–Grt–Sil–Qtz–Liq; 26) Bt–Pl–Grt–Crd–Ilm–Sil–Qtz–Liq; 27) Bt–Pl–Kfs–Grt–Crd–Ilm–Sil–Liq; 28) Bt–Pl–Kfs–Grt–Ilm–Sil–Qtz–Liq; 29) Ms–Pl–Kfs–Grt–Sil–Qtz; 30) Bt–Ms–Pl–Kfs–Grt–Sil–Liq; 31) Bt–Pl–Kfs–Grt–Sil–Crn–Liq. See text for details.

Fig. 4. Calculated mineral and melt abundance along prograde path (at 6 kbar) for various melt-reintegration scenarios of Figure 3 (El Hoyazo sample). Each vertical black line corresponds to a single melt-reintegration step as reported in Figure 3. See text for details.

Fig. 5. Melt-reintegration approach for residual migmatite MST45 (Mt. Stafford). Successive *P–T* pseudosection panels show from right to left the changes in the topology of the assemblage fields after each melt-reintegration step. The right-hand panel is always from the *P–T* pseudosection for the residuum composition. Labels reported above each panel refer to the bulk composition used for calculations (see Table 1). The chosen chemical system is NCKFMASHT. Red continuous line: solidus. Red dotted line: solidus for the residuum composition. Yellow continuous line: muscovite-out curve. Orange continuous line: biotite-out curve. Light blue field: region where liquid H₂O is predicted. (a, b, c) *P–T* pseudosections derived from melt-reintegration methods proposed in the literature (methods 2, 3 and 4, respectively). 1) Bt–Ms–Pl–Kfs–And–Qtz; 2) Bt–Pl–Kfs–Sill–Qtz–H₂O; 3) Bt–Pl–Kfs–Crd–Sill–Qtz–H₂O; 4) Bt–Pl–Kfs–Crd–Ilm–And–Qtz–H₂O; 5) Pl–Kfs–Crd–Ilm–Grt–Qtz–Liq; 6) Pl–Kfs–Crd–Ilm–Grt–Qtz; 7) Pl–Kfs–Crd–Grt–Ilm–Spl–Liq; 8) Pl–Kfs–Crd–Ilm–Spl–Liq; 9) Bt–Pl–Kfs–Crd–Grt–Ilm–Qtz–Liq. See text for details.

Fig. 6. Calculated mineral and melt abundance along prograde path (at 3.3 kbar) for various melt-reintegration scenarios of Figure 5 (Mt. Stafford sample). Each vertical black line corresponds to a single melt-reintegration step as reported in Figure 5. See text for details.

Fig. 7. Harker plots (wt.%) showing the trajectories for the evolving bulk rock compositions (El Hoyazo sample) as melt is reintegrated (anhydrous compositions from Table 1). Coloured dots: final protolith compositions. Empty dots: intermediate compositions. Grey area: compositional variability of metasedimentary rocks constituting the surrounding Alboran Sea basement and Alpujarride metamorphic complex. These rocks likely represent the protolith of El Hoyazo enclaves. Data from: Abad et al. (2003), Acosta-Vigil et al. (2001), Cesare et al., (1997), García-Casco & Torres-Roldán (1999), Ruiz Cruz et al. (2005, 2006), Ruiz Cruz & Sanz De Galdeano (2014), Spadea & Prosser (1999).

Fig. 8. Harker plots (wt.%) showing the trajectories for the evolving bulk rock compositions (Mt. Stafford sample) as melt is reintegrated (anhydrous compositions from Table 1). Coloured dots: final protolith compositions. Empty dots: intermediate compositions. Grey area: compositional variability of Zone 1 and Zone 2a metapelites. Data from: Greenfield (1997), Palya et al. (2011), Wang et al. (2014), and references therein.

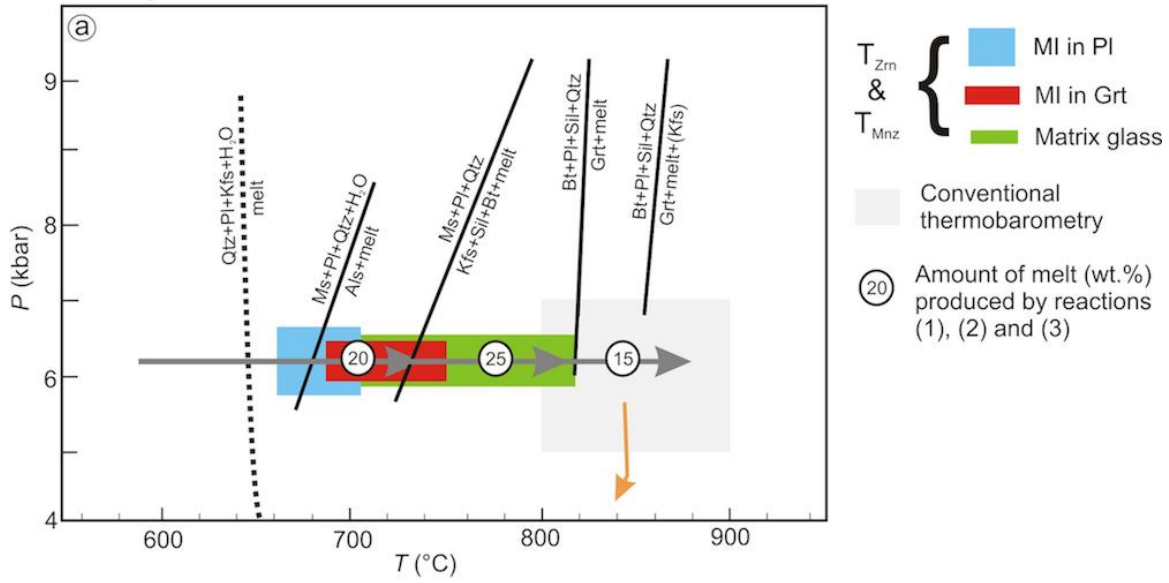
Fig. 9. Comparison of the melt productivity for the final model protolith compositions for El Hoyazo enclaves (a) and Mt. Stafford migmatites (b). Curves lighter in color in (a) correspond to values calculated in the Ti-bearing system. Bulk rock compositions used in the modelling are reported in parenthesis (see Table 1). See text for details.

TABLE CAPTIONS

Table 1. Bulk rock compositions (wt.%) used in the modelling.

Table 1. Bulk rock compositions (wt.%) used in the modeling.															
El Hoyazo															
	HO50	HO50d	HO50e	HO50f	HO50g	HO50h	HO50i	HO50j	HO50k	HO50l	HO50m	HO50n	HO50o	HO50p	HO50q
SiO ₂	45.37	48.04	51.93	54.45	50.19	45.81	46.53	46.76	46.94	47.59	48.61	46.30	47.44	48.52	49.50
TiO ₂	1.43	1.29	1.07	0.94	1.12	1.40	1.36	1.34	1.33	1.29	1.23	1.36	1.29	1.23	1.17
Al ₂ O ₃	29.91	28.27	25.61	23.87	26.93	29.64	29.19	29.05	28.92	28.45	27.71	29.35	28.64	27.95	27.23
FeO	13.24	11.98	10.06	8.89	10.70	13.01	12.66	12.54	12.42	12.07	11.51	12.72	12.16	11.61	11.07
MgO	2.13	1.92	1.57	1.38	1.71	2.09	2.03	2.01	1.99	1.94	1.85	2.04	1.95	1.86	1.77
CaO	2.37	2.17	1.87	1.66	1.96	2.33	2.27	2.26	2.24	2.18	2.09	2.28	2.19	2.10	2.01
Na ₂ O	2.68	2.73	2.87	2.85	2.91	2.70	2.72	2.73	2.74	2.76	2.80	2.75	2.78	2.82	2.85
K ₂ O	2.48	2.80	3.17	3.39	3.08	2.54	2.62	2.64	2.67	2.74	2.85	2.62	2.74	2.85	2.96
H ₂ O	0.39	0.81	1.85	2.56	1.41	0.49	0.63	0.68	0.75	0.98	1.36	0.58	0.81	1.06	1.43
Tot.	100	100	100	100	100	100	100	100	100	100	100	100	100	100	100
Mt. Stafford															
	MST45	MST45a	MST45b	MST45c	MST45d	MST45e	MST45f	MST45g	MST45h	MST45i	MST45j	MST16	MST16a	1107Pe	9115Pe
SiO ₂	55.50	58.74	55.67	56.62	57.07	57.22	58.17	56.30	57.06	57.80	58.46	50.50	52.52	69.23	58.94
TiO ₂	0.79	0.63	0.78	0.73	0.71	0.71	0.66	0.75	0.71	0.68	0.65	0.88	0.78	0.57	0.87
Al ₂ O ₃	24.61	22.46	24.50	23.86	23.55	23.45	22.80	24.08	23.57	23.08	22.61	30.11	28.58	17.38	21.10
FeO	8.27	6.98	8.20	7.82	7.63	7.55	7.07	7.96	7.65	7.32	6.98	8.86	7.92	4.92	7.77
MgO	2.97	2.43	2.94	2.79	2.71	2.68	2.51	2.84	2.71	2.58	2.46	3.18	2.82	1.71	2.75
CaO	0.16	0.20	0.16	0.17	0.17	0.17	0.17	0.17	0.18	0.18	0.18	0.07	0.13	0.18	0.33
Na ₂ O	1.54	1.78	1.55	1.63	1.67	1.69	1.81	1.60	1.66	1.74	1.83	0.61	0.80	0.53	0.98
K ₂ O	5.65	5.65	5.65	5.65	5.64	5.64	5.58	5.65	5.65	5.63	5.58	4.97	5.20	4.53	5.87
H ₂ O	0.50	1.13	0.53	0.73	0.84	0.89	1.22	0.64	0.81	1.00	1.26	0.82	1.26	0.96	1.39
Tot.	100	100	100	100	100	100	100	100	100	100	100	100	100	100	100

El Hoyazo



Mt. Stafford

